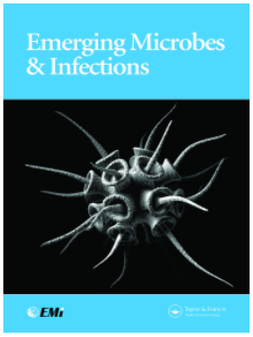

Emerging Microbes & Infections

ISSN: (Print) (Online) Journal homepage: https://www.tandfonline.com/loi/temi20

Identification of circulating microRNA profiles associated with pulmonary function and radiologic features in survivors of SARS-CoV-2-induced ARDS

María C. García-Hidalgo, Jessica González, Iván D. Benítez, Paola Carmona, Sally Santisteve, Manel Pérez-Pons, Anna Moncusí-Moix, Clara Gort-Paniello, Fátima Rodríguez-Jara, Marta Molinero, Thalia Belmonte, Gerard Torres, Gonzalo Labarca, Estefania Nova-Lamperti, Jesús Caballero, Jesús F. Bermejo-Martin, Adrián Ceccato, Laia Fernández-Barat, Ricard Ferrer, Dario Garcia-Gasulla, Rosario Menéndez, Ana Motos, Oscar Peñuelas, Jordi Riera, Antoni Torres, Ferran Barbé, David de Gonzalo-Calvo & on behalf of the CIBERESUCICOVID Project (COV20/00110 ISCIII)

To cite this article: María C. García-Hidalgo, Jessica González, Iván D. Benítez, Paola Carmona, Sally Santisteve, Manel Pérez-Pons, Anna Moncusí-Moix, Clara Gort-Paniello, Fátima Rodríguez-Jara, Marta Molinero, Thalia Belmonte, Gerard Torres, Gonzalo Labarca, Estefania Nova-Lamperti, Jesús Caballero, Jesús F. Bermejo-Martin, Adrián Ceccato, Laia Fernández-Barat, Ricard Ferrer, Dario Garcia-Gasulla, Rosario Menéndez, Ana Motos, Oscar Peñuelas, Jordi Riera, Antoni Torres, Ferran Barbé, David de Gonzalo-Calvo & on behalf of the CIBERESUCICOVID Project (COV20/00110 ISCIII) (2022): Identification of circulating microRNA profiles associated with pulmonary function and radiologic features in survivors of SARS-CoV-2-induced ARDS, Emerging Microbes & Infections, DOI: 10.1080/22221751.2022.2081615

To link to this article: https://doi.org/10.1080/22221751.2022.2081615

Publisher: Taylor & Francis & The Author(s). Published by Informa UK Limited, trading as Taylor & Francis Group, on behalf of Shanghai Shangyixun Cultural Communication Co., Ltd

Journal: *Emerging Microbes & Infections*

DOI: 10.1080/22221751.2022.2081615

Identification of circulating microRNA profiles associated with pulmonary function and radiologic features in survivors of SARS-CoV-2-induced ARDS

María C. García-Hidalgo,[1] Jessica González,[1,2] Iván D. Benítez,[1,2] Paola Carmona,[1] Sally Santisteve,[1] Manel Pérez-Pons,[1,2] Anna Moncusí-Moix,[1,2] Clara Gort-Paniello,[1,2] Fátima Rodríguez-Jara,[1] Marta Molinero,[1] Thalia Belmonte,[1,2] Gerard Torres,[1,2] Gonzalo Labarca,[3,4] Estefania Nova-Lamperti,[3] Jesús Caballero,[5] Jesús F. Bermejo-Martin,[2,6] Adrián Ceccato,[2] Laia Fernández-Barat,[2,7] Ricard Ferrer,[2,8] Dario Garcia-Gasulla,[9] Rosario Menéndez,[2,10] Ana Motos,[2,7] Oscar Peñuelas,[2,11] Jordi Riera,[2,8] Antoni Torres,[2,7] Ferran Barbé,[1,2] David de Gonzalo-Calvo,[1,2,*]

on behalf of the CIBERESUCICOVID Project (COV20/00110, ISCIII).

[1] Translational Research in Respiratory Medicine, University Hospital Arnau de Vilanova and Santa Maria, IRBLleida, Lleida, Spain.

[2] CIBER of Respiratory Diseases (CIBERES), Institute of Health Carlos III, Madrid, Spain.

[3] Molecular and Translational Immunology Laboratory, Department of Clinical Biochemistry and Immunology, Faculty of Pharmacy, Universidad de Concepcion, Concepcion, Chile.

[4] Internal Medicine Unit, Complejo Asistencial Dr. Víctor Ríos Ruiz, Los Ángeles, Chile.

[5] Intensive Care Department, University Hospital Arnau de Vilanova, IRBLleida, Lleida, Spain. [6] Hospital Universitario Río Hortega de Valladolid, Valladolid, Spain; Instituto de Investigación Biomédica de Salamanca (IBSAL), Salamanca, Spain.

[7] Servei de Pneumologia, Hospital Clinic; Universitat de Barcelona; IDIBAPS, Barcelona, Spain.

[8] Intensive Care Department, Vall d'Hebron Hospital Universitari. SODIR Research Group, Vall d'Hebron Institut de Recerca (VHIR), Spain.

[9] Barcelona Supercomputing Center (BSC), Barcelona, Spain.

[10] Pulmonology Service, University and Polytechnic Hospital La Fe, Valencia, Spain.

[11] Hospital Universitario de Getafe, Madrid, Spain.

Correspondence to:

David de Gonzalo-Calvo, Ph.D.

Translational Research in Respiratory Medicine, University Hospital Arnau de Vilanova and Santa Maria, IRBLleida.

Avda. Alcalde Rovira Roure 80 · 25198 Lleida, Spain.

E-mail: dgonzalo@irblleida.cat

Identification of circulating microRNA profiles associated with pulmonary function and radiologic features in survivors of SARS-CoV-2-induced ARDS

Abstract

There is a limited understanding of the pathophysiology of postacute pulmonary sequelae in severe COVID-19. The aim of current study was to define the circulating microRNA (miRNA) profiles associated with pulmonary function and radiologic features in survivors of SARS-CoV-2-induced ARDS. The study included patients who developed ARDS secondary to SARS-CoV-2 infection (n=167) and a group of infected patients who did not develop ARDS (n=33). Patients were evaluated 3 months after hospital discharge. The follow-up included a complete pulmonary evaluation and chest computed tomography. Plasma miRNA profiling was performed using RT-qPCR. Random forest was used to construct miRNA signatures associated with lung diffusing capacity for carbon monoxide (D_{LCO}) and total severity score (TSS). Kyoto Encyclopedia of Genes and Genomes (KEGG) and Gene Ontology (GO) enrichment analyses were conducted. D_{LCO}<80% predicted was observed in 81.8% of the patients. TSS showed a median [P_{25};P_{75}] of 5 [2;8]. The miRNA model associated with D_{LCO} comprised miR-17-5p, miR-27a-3p, miR-126-3p, miR-146a-5p and miR-495-3p. Concerning radiologic features, a miRNA signature composed by miR-9-5p, miR-21-5p, miR-24-3p and miR-221-3p correlated with TSS values. These associations were not observed in the non-ARDS

group. KEGG pathway and GO enrichment analyses provided evidence of molecular mechanisms related not only to profibrotic or anti-inflammatory states but also to cell death, immune response, hypoxia, vascularization, coagulation and viral infection. In conclusion, diffusing capacity and radiological features in survivors from SARS-CoV-2-induced ARDS are associated with specific miRNA profiles. These findings provide novel insights into the possible molecular pathways underlying the pathogenesis of pulmonary sequelae.

Keywords: acute respiratory distress syndrome; COVID-19; lung function; microRNA; sequelae; total severity score.

Introduction

Persistent pulmonary dysfunction has been described as a common clinical feature in survivors of acute respiratory distress syndrome (ARDS) [1,2]. Indeed, 15-50% of patients who recovered from ARDS as a consequence of coronavirus pneumonia, such as in severe acute respiratory syndrome (SARS) and Middle East respiratory syndrome (MERS), experienced major long-term sequelae after hospital discharge (3-24 months), including impaired lung diffusing capacity for carbon monoxide (D_{LCO}) and radiological abnormalities [3–5]. Our group recently demonstrated that up to 80% of survivors of ARDS secondary to SARS-CoV-2 infection showed diffusion impairment and pulmonary structural alterations in a 3-month follow-up study [6]. Similar findings have been reported in different cohorts of discharged COVID-19 patients [7–11].

Given the significant burden of pulmonary sequelae caused by SARS-CoV-2 and the current lack of evidence to treat lung dysfunction in "post-COVID" syndrome, the development of innovative therapies is of vital importance. In this scenario, molecular phenotyping of the patient emerges as an essential tool to identify the underlying biological factors implicated in the sequelae and, consequently, targets for intervention [12].

MicroRNAs (miRNAs) are single-stranded noncoding RNA sequences (19-25 nt) that function as posttranscriptional repressors of gene expression. miRNAs participate in complex and coordinated regulatory networks [13], with a single miRNA regulating large sets of genes and a single gene able to be targeted by large sets of miRNAs. This

biological system allows the fine-tuning of the cellular phenotype. As such, miRNAs constitute essential modulators of cellular development, homeostasis and response to stress [14]. miRNAs have also been described in the extracellular space [15], including biofluids such as plasma [16]. Extracellular miRNAs could act as signaling molecules at the paracrine and endocrine levels to regulate a broad array of physiological processes [17,18]. Their aberrant expression plays a significant role in the onset and development of pathological conditions, including pulmonary diseases [19,20].

Here, we evaluated the association between pulmonary function and radiologic features and the circulating miRNA profile in survivors of SARS-CoV-2-induced ARDS 3 months after hospital discharge. The final aim is to decipher the pathophysiology of the postacute pulmonary sequelae of severe COVID-19. To the best of our knowledge, this is the first study that uses an approach based on the miRNA transcriptome to characterize the pulmonary function and structural outcomes of ARDS secondary to SARS-CoV-2 infection.

Methods

Ethics statements

The study protocol was approved by the medical ethics committee of Hospital Universitari Arnau de Vilanova (CEIC/2273) and the Institutional Review Board (IRB) from Servicio de Salud Bio (IRB: CEC113) and Servicio de Salud Concepcion (IRB: CEC-SSC: 20-07-26). The study protocol was registered in the ISRCTN registry (ID: ISRCTN16865246). The study was performed in full compliance with the Declaration of Helsinki. The patients received written information about the nature and goals of the study and signed an informed consent form. Patient data and sample data are kept in a database with restricted access.

Study design and population

This is a substudy of the ongoing multicenter study CIBERESUCICOVID registered at www.clinicaltrials.gov with the identification NCT04457505 [21]. This was a prospective study including patients admitted due to severe COVID-19 at Hospital Universitari Arnau de Vilanova-Santa María (Lleida, Spain) between March and December 2020. Patients were evaluated in a "post-COVID" consultation 3 months after hospital discharge in the same hospital (median [P_{25};P_{75}] of 96.00 [85.75;107.00] days). The final study population was selected according to the following inclusion criteria: i) positive for SARS-CoV-2 according to a standardized test; ii) aged over 18; iii) developed ARDS according to the Berlin definition [22] during hospital stay; and iv) attended a "post-COVID" consultation. The exclusion criteria for the "Post-COVID" evaluation were: i) less than 1 year of life expectancy; ii) transferred to another institution; iii) treated with palliative care; and iv) impossible to evaluate performance due to severe mental disability. A control group composed by patients positive for SARS-CoV-2 but who did not develop ARDS was additionally included. Patients were evaluated at Hospital Universitari Arnau de Vilanova-Santa María (Lleida, Spain), Hospital Complejo Víctor Ríos Ruiz (Los Ángeles, Chile) and Hospital Guillermo Grant Benavente (Concepción, Chile) between July 2020 and August 2021. Demographic, clinical, pharmacological and laboratory data were abstracted from the electronic medical records and entered into a REDCap database.

Pulmonary evaluation

A complete pulmonary evaluation was performed as previously described [6]. Airway function was measured using a flow spirometer (MasterScreen, Jaeger, Germany)

according to the guidelines of the American Thoracic Society [23]. The results were expressed as a percentage of the D_{LCO} predicted value according to the European Community Lung Health Survey [24] Chest computed tomography (CT) examinations were performed using a sixteen- and sixty-four-slice multidetector CT scanner (Brilliance 16 and 64; Philips Healthcare). Images were acquired with patients in the supine position in the cranio-caudal direction at end-inspiration. To quantify the severity of lung affectation, the total severity score (TSS) was assessed. Each of the five lung lobes was determined for the percentage of lobar involvement. Following this, the severity of each lobe was classified as none (0%), minimal (1-25%), mild (26-50%), moderate (51-75%), or severe (76-100%), with a corresponding score of 0, 1, 2, 3 or 4, respectively. The TSS is calculated by summing the five lobe scores (range from 0 to 20) [25].

Samples

Samples collected at the Hospital Universitari Arnau de Vilanova-Santa María (Lleida, Spain) were processed in standardized conditions with support by IRBLleida Biobank (B.0000682) and "Plataforma Biobancos PT20/00021". Samples collected at the University of Concepción (Concepción, Chile) were processed using standardized conditions according to international Biobank regulations. Venous blood samples were obtained in ethylenediaminetetraacetic acid (EDTA) blood collection tubes (BD, NJ, USA) by venipuncture after a night of fasting and before beginning any interventional procedure at the "post-COVID" consultation 3 months after hospital discharge. To obtain plasma, blood samples were fractionated by centrifugation at 1,500 xg for 10 minutes at room temperature. After centrifugation, the plasma supernatant was immediately aliquoted, frozen and stored at -80°C until analysis. Samples collected in University of Concepción (Concepción, Chile) were shipped on dry ice to the IRBLleida Biobank.

Antigen detection in plasma

Panbio® COVID-19 Ag Rapid Test Device (Abbott, Chicago, IL, USA) was used to detect the N antigen of SARS-CoV-2 in the plasma samples.

microRNA quantification

RNA isolation and miRNA quantification were conducted in the same laboratory using standardized protocols. Experienced staff blinded to patient data performed the miRNA quantification.

Total RNA was isolated from 200 µL of frozen plasma using the miRNeasy Serum/Plasma Advanced kit (Qiagen, Hilden, Germany) according to the manufacturer's instructions. For normalization, synthetic *Caenorhabditis elegans* miR-39-3p (cel-miR-39-3p), lacking sequence homology to human miRNAs, was added as an external reference miRNA (1.6×10^8 copies/µL). The mixture was supplemented with 1 µg of MS2 carrier RNA (Roche Diagnostics, Mannheim, Germany), not containing miRNAs, to improve extracellular miRNA yield. The RNA Spike-In Kit (UniSp2, UniSp4 and UniSp5) (Qiagen, Hilden, Germany) was added to monitor RNA isolation. All reagents were spiked into samples during RNA isolation after incubation with the denaturing solution. RNA was eluted with 20 µL of RNAse-free water and stored at -80°C.

miRNA quantification was performed according to the protocol from the miRCURY LNA Universal RT microRNA PCR System (Qiagen, Hilden, Germany), which offers optimal analytical performance [26]. Reverse transcription (RT) cDNA synthesis was performed using a miRCURY LNA RT Kit (Qiagen, Hilden, Germany) in a total reaction volume of 10 µL. An additional spike-in UniSp6 (Qiagen, Hilden, Germany) was added to monitor the RT reaction. The RT reactions were performed under

the following conditions: incubation for 60 minutes at 42°C, inactivation for 5 minutes at 95°C, and immediate cooling to 4°C. Then, cDNA was stored at 20°C. A panel of 41 miRNAs **(Supplemental Table S1)**, previously described [27], was analyzed using miRCURY LNA miRNA Custom Panels (384-well plates) (Qiagen, Hilden, Germany). qPCR was carried out using the QuantStudio™ 7 Flex Real-Time PCR System (Applied Biosystems, Waltham, MA, USA) in a total volume of 10 μL. RT-qPCR conditions were 95°C for 2 minutes, followed by 40 cycles of 95°C for 10 seconds and 56°C for 1 minute, followed by melting curve analysis. Synthetic UniSp3 was analyzed as an interplate calibrator and qPCR control. Amplification curves were evaluated using QuantStudio Software v1.3 (Thermo Fisher Scientific, Massachusetts, USA).

The quantification cycle (Cq) was defined as the fractional cycle number at which the fluorescence exceeded a given threshold. The specificity of the qPCR was corroborated by melting curve analysis. To ensure the optimal quality of the data, the spike-in RNA templates were first analyzed to monitor the uniformity of the RNA extraction procedure and the efficiency of the RT and PCR. Hemolysis contamination was excluded as previously described [28]. miRNAs were considered to be expressed at Cq values < 35. Cqs above 35 cycles were considered undetectable and were censored at the minimum level observed for each miRNA. Relative quantification was performed using the $2^{-\Delta Cq}$ method ($\Delta Cq = Cq_{miRNA}-Cq_{cel\text{-}miR\text{-}39\text{-}3p}$). Expression levels were log-transformed for statistical purposes.

Molecular pathway and Gene Ontology analyses

Bioinformatic prediction analysis was performed using the web-based computational tool DIANA-miRPath v3.0 [29]. DIANA-miRPath v3.0 combines information on manually curated experimentally validated miRNA:gene interactions

from TaRBase v7.0 with the Kyoto Encyclopedia of Genes and Genomes (KEGG) database and Gene Ontology (GO) annotations (for biological processes). Enrichment analysis was performed using Fisher's exact test (hypergeometric distribution). The false discovery rate (FDR)-adjusted p-value was set at <0.05. A Venn diagram was generated to represent shared and unique molecular pathways and biological processes for pulmonary function and radiologic features.

Statistical analysis

Descriptive statistics were used to summarize the characteristics of the study population. Data are presented as the median [P_{25};P_{75}] for continuous variables and as frequencies (percentage) for categorical variables. Due to the high burden of diffusion impairment and the lack of clinical cutoff for radiological features, both D_{LCO} and TSS were analyzed as tertiles and/or continuous variables. To identify a dose-response relationship between individual miRNAs and the outcomes, differential expression was based on p for trend using linear models for arrays [30]. The models included miRNA levels as outcome and study variables categorized by tertiles (transformed as: first tertile = 1; second tertile = 2; third tertile = 3). Differential expression between study groups is displayed in volcano plots. The multivariable analysis was performed using random forest (RF). D_{LCO} and TSS were considered as continuous variables. The stepwise feature selection process for the random forest (RF) [31] was based on three steps [31,32]. First, elimination of variables with low importance by ranking the average of the variable importance measure on 50 runs of RF. Second, calculation of the Out-of-bag (OOB) error rates of 50 RF runs for each nested model (from the most important variable to the model with all variables previously selected). The variables included in the model with the lowest OOB error were selected. Third, selection of the final model by performing an

ascending sequence of RF that tests the inclusion of each variable selected in the second step. The relationship between the selected miRNAs and the outcomes was evaluated using generalized additive models (GAMs) with penalized cubic regression splines. The same models were used to adjust miRNA levels for age, sex, previous pulmonary disease, smoking history and the use of corticoids after hospital discharge. A sparse inverse covariance matrix using a Lasso (L1) penalty was estimated to study the correlation between miRNAs selected [33]. Correlations between continuous variables were estimated using Spearman rank correlation. Point-biserial correlations were used to calculate the correlations between dichotomous and continuous variables. The p-value threshold defining statistical differential expression was set at <0.05. All statistical analyses were performed using R software, version 4.0.2.

Results

Clinical characteristics of the patients

The study flowchart is presented in **Supplemental Figure S1**. Finally, 157 patients with ARDS secondary to SARS-CoV-2 infection and 33 patients who did not develop ARDS were available for miRNA quantification. Three samples were discarded due to insufficient plasma volume, the presence of hemolysis or low quality **(Supplemental Figure S2A & S2B)**. Five miRNAs, miR-34b-5p, miR-34c-5p, miR-124-3p, miR-208a-3p and miR-208b-3p, were not considered in the subsequent analysis due to undetectable levels in more than 80% of the samples.

Table 1 displays the characteristics of the study population. The median [P_{25};P_{75}] age was 61 [53.2;66.8], and females represented 30.5% of the population. D_{LCO} was abnormal (<80% predicted) in 81.8% of the population. The TSS score showed a median

[P_{25};P_{75}] of 5 [2;8]. The characteristics of the non-ARDS control groups are shown in **Supplemental Table S2**.

microRNA profiling of the pulmonary function

The characteristics of the study population according to D_{LCO} tertiles are detailed in **Table 2.** Patients with low D_{LCO} levels were older and had longer hospital and ICU stays, higher requirements for prone positioning and a higher lung affectation in the chest CT **(Table 2 & Supplemental Figure S3)**.

In univariate analyses, pulmonary function (as D_{LCO} tertiles) was inversely associated with levels of miR-146a-5p [fold change (FC) = 0.849] **(Figure 1A)**. RF selected a miRNA profile associated with D_{LCO} levels (as continuous variable) composed of five miRNAs: miR-17-5p, miR-27a-3p, miR-126-3p, miR-146a-5p and miR-495-3p **(Figure 1B)**. miRNAs established a dense correlation network **(Figure 1C)**. The individual relation between D_{LCO} levels and the plasma miRNAs selected was analyzed using GAM modeling. miR-17-5p, miR-27a-3p and miR-146a-5p were inversely and lineally associated with D_{LCO} **(Figure 1D)**; high levels of these three miRNAs correlated with low to very low levels of D_{LCO}, i.e., diffusion impairment. Similar results were observed after adjustment for confounders: age, sex, previous pulmonary disease, smoking history and the use of corticoids after hospital discharge **(Supplemental Figure S4A)**. These associations were not observed in non-ARDS patients positive for SARS-CoV-2 **(Supplemental Figure S5A)**. No correlation was observed between miRNA levels and invasive mechanical ventilation (IMV) duration or hospital and ICU stays **(Supplemental Figure S6)**.

Pathway and GO term enrichment analyses were performed to further understand the biological implications of the miRNA profiles described. Sixty-one KEGG pathways

and one hundred and fifty-one GO terms were enriched in experimentally validated target genes of the miRNAs that composed the signature **(Supplemental Tables S3 and S4)**. The analyses identified molecular pathways and biological processes related to fibrosis (e.g., TGF-beta signaling pathway, mTOR signaling pathway, Fibroblast growth factor receptor signaling pathway), inflammation and immune response (e.g., Leukocyte transendothelial migration, TNF signaling pathway, several Toll-like receptor signaling pathways, Type I interferon signaling pathway, Cytokine-mediated signaling pathway, Leukocyte migration), cell death (e.g., Apoptotic signaling pathway), hypoxia (e.g., HIF-1 signaling pathway, Cellular response to hypoxia), vascularization (e.g., Notch signaling pathway) and coagulation (e.g., Platelet activation, Blood coagulation, Platelet degranulation) **(Figure 1E & 1F)**. Several molecular GO terms linked to viral infections were also identified (e.g., Viral process, Viral life cycle, Viral transcription, Positive regulation of viral transcription, Response to virus) **(Figure 1E & 1F)**.

microRNA profiling of the radiologic features

A similar workflow was used to analyze the relation between the radiologic features and the circulating miRNA profile. **Table 3** shows the characteristics of the study population according to TSS tertiles. Higher levels of TSS were directly associated with age, monocyte count, creatinine and urea levels at hospital admission, hospital stay, ICU stay, the use of IMV, IMV duration, use of prone positioning, and prone positioning duration **(Table 3 & Supplemental Figure S7)**.

In univariate analyses, miR-9-5p [FC=0.823], miR-16-5p [FC=0.876] and miR-221-3p [FC=0.864] were inversely associated with TSS (as tertiles) **(Figure 2A)**. Following the same approach, the feature selection procedure constructed a signature composed of four miRNAs: miR-9-5p, miR-21-5p, miR-24-3p and miR-221-3p (using

TSS as continuous variable) **(Figure 2B)**. Except for miR-9-5p, which was poorly correlated with miR-221-3p, all miRNAs correlated with each other **(Figure 2C)**. GAM modeling showed that low levels of both miR-9-5p and miR-24-3p adjusted to an inverse linear relation with TSS and, consequently, higher levels of radiologic abnormalities. A nonlinear relationship was observed for miR-21-5p and miR-221-3p **(Figure 2D)**. Confounding factors showed no significant impact on the miRNA-TSS relationship **(Supplemental Figure S4B)**. Except for miR-24-3p, the relationship between TSS levels and the selected miRNAs was only observed in the ARDS group **(Supplemental Figure S5B)**. Again, no correlation was observed between IMV duration or hospital and ICU stays and miRNA levels **(Supplemental Figure S6)**.

Forty-two KEGG pathways and 115 GO terms contained experimentally validated miRNA:gene interactions **(Supplemental Tables S5 and S6)**. Again, the analyses identified molecular pathways and biological processes related to fibrosis (e.g., TGF-beta signaling pathway, Fibroblast growth factor receptor signaling pathway), inflammation and immune response (e.g., TNF signaling pathway, several Toll-like receptor signaling pathways, Leukocyte migration), cell death (e.g., Apoptotic signaling pathway), hypoxia (e.g., HIF-1 signaling pathway, Cellular response to hypoxia), vascularization (e.g., Notch signaling pathway) and coagulation (e.g., Blood coagulation, Platelet degranulation, Platelet activation) and viral infections (e.g., Viral process, Viral life cycle, Viral transcription) **(Figure 2E & 2F)**. An overlap between those molecular pathways and GO terms enriched in targets from the miRNA signatures associated with lung function and radiologic features was observed **(Figure 3)**.

Molecular mechanisms involved in viral infection and response were highly enriched among the identified GO terms for both signatures. Therefore, we evaluated the

presence of viral antigens in plasma samples from a subset of 50 survivors of SARS-CoV-2-induced ARDS. Antigenemia was presented in two patients **(Supplemental Figure S8)**.

Discussion

Current study combined experimental and computational approaches to first evaluate the association between lung function and radiologic features and the circulating miRNA profile in survivors of SARS-CoV-2-induced ARDS 3 months after hospital discharge and then decipher the molecular mechanisms implicated in pulmonary outcomes. We report four major findings: i) distinct miRNA profiles are associated with pulmonary function and radiologic features; ii) this association seems to be specific for ARDS secondary to SARS-CoV-2 infection; iii) pulmonary function and structural features are linked not only to mechanisms such as fibrosis or inflammation but also to cell death, immune response, hypoxia, vascularization, coagulation and viral infection; iv) as such, the mechanisms linked to the respiratory sequelae of SARS-CoV-2-induced ARDS might implicate multiple biological pathways.

Individual miRNAs have a modest impact on the regulation of biological processes [34]. Collective and coordinated miRNA expression networks, rather than single miRNAs, are critical for the regulation of the cellular phenotype [13]. The analysis of miRNA profiles is paramount. Furthermore, the deregulation in individual expression programs may not explain the complexity of the disease. For instance, Barbagallo et al. [35] have recently demonstrated a profound perturbation in competitive endogenous RNA networks due to SARS-CoV-2 infection which ultimately impacts on disease progression. Advanced statistical tools seem fundamental to describe the interaction between miRNAs and the phenotype and identify nonlinear associations between miRNA levels and the

outcome. Consequently, we constructed miRNA signatures using machine learning models. RF-based predictive models identified two miRNA signatures associated with pulmonary function and radiologic features in survivors of ARDS secondary to SARS-CoV-2 infection. The current results could improve the limited understanding of sequelae in survivors of SARS-CoV-2-induced ARDS. Supporting the significant functional redundancy among miRNAs [36], although the individual miRNAs that composed the patterns were different, the downstream regulatory effects were highly similar with miR-17-5p, miR-27a-3p, miR-126-3p, miR-146a-5p and miR-495-3p for D_{LCO} and miR-9-5p, miR-21-5p, miR-24-3p and miR-221-3p for TSS.

As expected, both pulmonary function and radiological features were closely linked to fibrotic and inflammatory pathways. The reduction in miR-9-5p, a suppressor of TGF-β1-dependent myofibroblast phenotypic transformation in lung disease [37], may indicate a profibrotic state in survivors of severe forms of COVID-19. The results in subjects with persistent symptoms after acute COVID-19 [38] and bioinformatic prediction using experimentally validated miRNA interactions corroborated this notion. Different cellular pathways related to fibrotic mechanisms in lung conditions were identified, including the AMPK signaling pathway [39], Hippo signaling pathway [40] and mTOR signaling pathway [41]. Concerning inflammation, multiple KEGG pathways and GO terms, such as signaling pathways involving TNF or Toll-like receptors, were enriched in the target genes of the miRNA patterns. More specifically, the levels of miR-146a-5p were closely and inversely associated with lung function. This miRNA is induced in response to proinflammatory cytokines and participates in a negative feedback regulation loop to control inflammation [42]. Therefore, its increase in survivors with higher pulmonary impairment may constitute an anti-inflammatory response to the extensive inflammatory insult inherent to the pathogenesis of ARDS, similar to the

production of anti-inflammatory cytokines in proinflammatory conditions. In fact, hypercytokinemia is a characteristic feature of severe COVID-19 [43], and its prolongation even 40-60 days postviral infection has been reported [44]. The biological functions of the other miRNAs that composed the signatures support this hypothesis. *In vitro* and *in vivo* approaches suggest that mesenchymal stem cell-derived extracellular vesicles mitigate acute lung injury at least partially by transferring miR-27a-3p to alveolar macrophages, a regulator of NFKB1 and M2 macrophage polarization [45]. Endothelial progenitor cell exosomes reduce local inflammatory cytokines in a model of lipopolysaccharide-induced acute lung injury, in part through the delivery of miR-126 [46].

The circulating miRNA signature may be informative about other driving factors that mediate sequelae from SARS-CoV-2-induced ARDS. KEGG and GO analyses highlighted pathways related to platelet function and blood coagulation. SARS-CoV-2 infection induces a pro-coagulant state that has been recognized as a hallmark of COVID-19 [47]. We have previously demonstrated alterations in the circulating profile of miRNAs implicated in coagulation mechanisms during the acute phase of the disease [27]. According to our findings, the pathways related to the coagulation process remain perturbed even 3 months after hospital discharge. Although the clinical relevance remains uncertain [48], these results are in line with the occurrence of thrombotic events after discharge or resolution of infection [49]. In addition, miRNA signatures were enriched in targets of signaling pathways implicated in cell death/apoptosis (e.g., FoxO signaling pathway or p53 signaling pathway, among others), indicating that the cell injury mechanisms modulated during the acute phase by SARS-CoV-2 [50] are still deregulated in "post-COVID" syndrome. Interestingly, the increased level of miR-126-3p in patients with significant diffusion impairment is compatible with aberrant angiogenic signaling.

Cao et al. [51] recently demonstrated that miR-126-3p inhibits the angiogenic function of human lung microvascular endothelial cells, which are essential for gas exchange and for lung injury repair and regeneration. Current results may have a relevant impact, since the mechanisms that mediate microvascular injury in ARDS sequelae are uncertain [52]. Possible evidence for the phenotypic implications of our findings is given by the identification of target genes in hypoxia signaling pathways. The perturbations in these mechanisms may explain the decreased average, final and minimal oxygen saturation in the 6-minute walking test that we have previously described in survivors of SARS-CoV-2-induced ARDS [6]. Of note, the miRNA signatures were also enriched in targets from GO terms related to viral infection. Despite this fact, we have not detected the virus in the blood through antigenemia profiling. A plausible explanation is the presence of viral fragments in other tissues causing immunoreactivity and persistent inflammation [53]. The alteration of these biological processes during the recovery phase deserves additional investigation.

Although the endocrine function of circulating miRNAs is still not completely elucidated [54], our work suggests a potential role of miRNAs in the respiratory sequelae of severe COVID-19. Overall, the current results provide a framework for targeted interventions against the sequelae of patients who develop SARS-CoV-2-induced ARDS. The management of the long-lasting effects of this syndrome should be based on a comprehensive and multidisciplinary approach to not only focus on inflammation and fibrosis but also other relevant pathological processes.

Our results should be considered in the context of several limitations. First, survivors of ARDS secondary to SARS-CoV-2 infection were recruited in a single center. The results should be validated in independent cohorts. Second, potential confounding due to previous comorbidities, clinical management and inpatient complications should

not be discarded. Third, how the deregulation of the miRNA signature in plasma impacts the pulmonary sequelae remains to be elucidated. Further functional studies may provide additional insights into role of the miRNAs in pulmonary abnormalities. Forth, we used a targeted approach using miRNAs previously associated with COVID-19 and/or pathological mechanisms linked to COVID-19/ARDS [27]. Other miRNAs could be associated with pathophysiology of the postacute pulmonary sequelae. Large-scale miRNA analyses are fundamental. Fifth, potential overfitting should be acknowledged. In addition, the impact of type I error should not be discarded.

In conclusion, the pulmonary function and radiologic features in survivors of ARDS secondary to SARS-CoV-2 infection are associated with specific plasma miRNA patterns. The multifactorial mechanisms linked to the miRNA profiles provide novel knowledge of the physiopathology of persistent pulmonary dysfunction in the recovery stage and, in consequence, further insights into postacute care strategies.

Acknowledgments

The authors are indebted to María Arguimbau, Raquel Campo, Natalia Jarillo, Javier Muñoz and Manuel Sánchez(†) for their extensive support with project management and article preparation. This work was supported by IRBLleida Biobank (B.0000682) and “Plataforma Biobancos PT20/00021". The human sample manipulation was performed in the Cell Culture Technical Scientific Service of the Universitat de Lleida (Lleida, Catalonia, Spain). The authors acknowledge all the COVID-19 patients and health workers involved in the study.

Funding

This work is supported by Instituto de Salud Carlos III (COV20/00110), co-funded by European Regional Development Fund (ERDF)/"A way to make Europe". CIBERES is an initiative of the Instituto de Salud Carlos III. CIBERES is an initiative of the Instituto de Salud Carlos III. Suported by: Programa de donaciones "estar preparados" UNESPA (Madrid, Spain) and Fundación Francisco Soria Melguizo (Madrid, Spain).. Finançat per La Fundació La Marató de TV3, projecte amb codi 202108-30/-31. COVIDPONENT is funded by Institut Català de la Salut and Gestió de Serveis Sanitaris. MM is the recipient of a predoctoral fellowship (PFIS: FI21/00187) from Instituto de Salud Carlos III. MCGH is the recipient of a predoctoral fellowship from "University of Lleida". DdGC has received financial support from Instituto de Salud Carlos III (Miguel Servet 2020: CP20/00041), co-funded by the European Social Fund (ESF)/"Investing in your future". ENL and GL were funded by COVID1005 and ACT210085 from National Agency of Investigation & Development (ANID), Chile.

Disclosure

DdGC holds patents on microRNAs as biomarkers. The other authors declare that they have no competing interests.

References

[1] Masclans J, Roca O, Muñoz X, et al. Quality of life, pulmonary function, and tomographic scan abnormalities after ARDS. Chest. 2011;139:1340–1346.

[2] Heyland D, Groll D, Caeser M. Survivors of acute respiratory distress syndrome:

relationship between pulmonary dysfunction and long-term health-related quality of life. Crit Care Med. 2005;33:1549–1556.

[3] Ngai JC, Ko FW, Ng SS, et al. The long-term impact of severe acute respiratory syndrome on pulmonary function, exercise capacity and health status. Respirology. 2010;15:543–550.

[4] Ahmed H, Patel K, Greenwood DC, et al. Long-term clinical outcomes in survivors of severe acute respiratory syndrome (SARS) and Middle East respiratory syndrome (MERS) coronavirus outbreaks after hospitalisation or ICU admission: A systematic review and meta-analysis. J. Rehabil. Med. 2020. p. 52: jrm00063.

[5] Hui D, Joynt G, Wong KT, et al. Impact of severe acute respiratory syndrome (SARS) on pulmonary function, functional capacity and quality of life in a cohort of survivors. Thorax. 2005;60:401–409.

[6] González J, Benítez ID, Carmona P, et al. Pulmonary Function and Radiologic Features in Survivors of Critical COVID-19. Chest. 2021;160:187–198.

[7] van Gassel RJJ, Bels JLM, Raafs A, et al. High prevalence of pulmonary sequelae at 3 months after hospital discharge in mechanically ventilated survivors of COVID-19. Am J Respir Crit Care Med. 2021;203:371–374.

[8] Blanco JR, Cobos-Ceballos MJ, Navarro F, et al. Pulmonary long-term consequences of COVID-19 infections after hospital discharge. Clin Microbiol Infect. 2021;

[9] Huang C, Huang L, Wang Y, et al. 6-month consequences of COVID-19 in patients discharged from hospital: a cohort study. Lancet. 2021;397:220–232.

[10] Guler S, Ebner L, Aubry-Beigelman C, et al. Pulmonary function and radiological features 4 months after COVID-19: first results from the national prospective observational Swiss COVID-19 lung study. Eur Respir J. 2021;57:2003690.

[11] Sibila O, Albacar N, Perea L, et al. Lung Function sequelae in COVID-19 Patients 3 Months After Hospital Discharge. Arch Bronconeumol. 2021;57:59–61.

[12] García-Hidalgo MC, González J, Benítez ID, et al. Proteomic profiling of lung diffusion impairment in the recovery stage of SARS-CoV-2- induced ARDS. Clin Transl Med. 2022; 10.1002/ctm2.838.

[13] Ebert MS, Sharp PA. Roles for MicroRNAs in conferring robustness to biological processes [Internet]. Cell. Elsevier B.V.; 2012 [cited 2021 Jun 17]. p. 515–524.

[14] Mendell J, Olson E. MicroRNAs in stress signaling and human disease. Cell. 2012;148:1172–1187.

[15] Valadi H, Ekström K, Bossios A, et al. Exosome-mediated transfer of mRNAs and microRNAs is a novel mechanism of genetic exchange between cells. Nat Cell Biol. 2007;9:654–659.

[16] Mitchell P, Parkin R, Kroh E, et al. Circulating microRNAs as stable blood-based markers for cancer detection. Proc Natl Acad Sci U S A. 2008;105:10513–10518.

[17] Mori M, Ludwig R, Garcia-Martin R, et al. Extracellular miRNAs: From Biomarkers to Mediators of Physiology and Disease. Cell Metab. 2019;30:656–673.

[18] Cheng M, Yang J, Zhao X, et al. Circulating myocardial microRNAs from infarcted hearts are carried in exosomes and mobilise bone marrow progenitor cells. Nat Commun. 2019;10:959.

[19] Gomez I, Ward B, Souilhol C, et al. Neutrophil microvesicles drive atherosclerosis by delivering miR-155 to atheroprone endothelium. Nat Commun. 2020;11:214.

[20] Holtzman J, Lee H. Emerging role of extracellular vesicles in the respiratory system. Exp Mol Med. 2020;52:887–895.

[21] Torres A, Arguimbau M, Bermejo-Martín J, et al. CIBERESUCICOVID: un

proyecto estratégico para una mejor comprensión y manejo clínico de la COVID-19 en pacientes críticos. Arch Bronconeumol. 2021;57:1–2.

[22] Ranieri VM, Rubenfeld GD, Thompson BT, et al. Acute respiratory distress syndrome: The Berlin definition. JAMA - J Am Med Assoc. 2012;307:2526–2533.

[23] Celli BR, MacNee W, Agusti A, et al. Standards for the diagnosis and treatment of patients with COPD: a summary of the ATS/ERS position paper. Eur Respir J. 2004;23:932–946.

[24] Roca J, Burgos F, Sunyer J, et al. References values for forced spirometry. Group of the European Community Respiratory Health Survey. Eur Respir J. 1998;11:1354–1362.

[25] Ooi GC, Khong PL, Müller NL, et al. Severe acute respiratory syndrome: temporal lung changes at thin-section CT in 30 patients. Radiology. 2004;230:836–844.

[26] Mestdagh P, Hartmann N, Baeriswyl L, et al. Evaluation of quantitative miRNA expression platforms in the microRNA quality control (miRQC) study. Nat Methods. 2014;11:809–815.

[27] de Gonzalo-Calvo D, Benítez ID, Pinilla L, et al. Circulating microRNA profiles predict the severity of COVID-19 in hospitalized patients. Transl Res. 2021;S1931-5244:00122–00125.

[28] Blondal T, Jensby Nielsen S, Baker A, et al. Assessing sample and miRNA profile quality in serum and plasma or other biofluids. Methods. Academic Press Inc.; 2013. p. S1–S6.

[29] Vlachos IS, Zagganas K, Paraskevopoulou MD, et al. DIANA-miRPath v3.0: deciphering microRNA function with experimental support. Web Serv issue Publ online. 2015;43.

[30] Ritchie ME, Phipson B, Wu D, et al. limma powers differential expression analyses

for RNA-sequencing and microarray studies. Nucleic Acids Res. 2015;43:e47–e47.

[31] Breiman L. Random Forests. Mach Learn 2001 451. 2001;45:5–32.

[32] Genuer R, Poggi JM, Tuleau-Malot C. Variable selection using random forests. Pattern Recognit Lett. 2010;31:2225–2236.

[33] Friedman J, Hastie T, Tibshirani R. Sparse inverse covariance estimation with the graphical lasso. Biostatistics. 2007;9:432–441.

[34] Baek D, Villén J, Shin C, et al. The impact of microRNAs on protein output. Nature. 2008;455:64–71.

[35] Barbagallo D, Palermo CI, Barbagallo C, et al. Competing endogenous RNA network mediated by circ_3205 in SARS-CoV-2 infected cells. Cell Mol Life Sci. 2022;79:75.

[36] Miska EA, Alvarez-Saavedra E, Abbott AL, et al. Most Caenorhabditis elegans microRNAs Are Individually Not Essential for Development or Viability. PLOS Genet. 2007;3:e215.

[37] Fierro-Fernández M, Busnadiego Ó, Sandoval P, et al. miR-9-5p suppresses pro-fibrogenic transformation of fibroblasts and prevents organ fibrosis by targeting NOX 4 and TGFBR 2 . EMBO Rep. 2015;16:1358–1377.

[38] Chun HJ, Coutavas E, Pine AB, et al. Immuno-fibrotic drivers of impaired lung function in post-acute sequelae of SARS-CoV-2. JCI Insight. 2021;6:e148476.

[39] Kheirollahi V, Wasnick RM, Biasin V, et al. Metformin induces lipogenic differentiation in myofibroblasts to reverse lung fibrosis. Nat Commun. 2019;10:1–16.

[40] Gokey JJ, Sridharan A, Xu Y, et al. Active epithelial Hippo signaling in idiopathic pulmonary fibrosis. JCI insight. 2018;3:e98738.

[41] Platé M, Guillotin D, Chambers RC. The promise of mTOR as a therapeutic target pathway in idiopathic pulmonary fibrosis. Eur Respir Rev. 2020;29:200269.

[42] Taganov KD, Boldin MP, Chang K-J, et al. NF-κB-dependent induction of microRNA miR-146, an inhibitor targeted to signaling proteins of innate immune responses. Proc Natl Acad Sci. 2006;103:12481–12486.

[43] McElvaney OJ, McEvoy NL, McElvaney OF, et al. Characterization of the Inflammatory Response to Severe COVID-19 Illness. Am J Respir Crit Care Med. 2020;202:812–821.

[44] Heywood WE, Doykov I, Hällqvist J, et al. "The long tail of Covid-19" - The detection of a prolonged inflammatory response after a SARS-CoV-2 infection in asymptomatic and mildly affected patients. F1000Research. 2021;9:1349.

[45] Wang J, Huang R, Xu Q, et al. Mesenchymal Stem Cell-Derived Extracellular Vesicles Alleviate Acute Lung Injury Via Transfer of miR-27a-3p∗. Crit Care Med. 2020;48:E599–E610.

[46] Zhou Y, Li P, Goodwin AJ, et al. Exosomes from endothelial progenitor cells improve outcomes of the lipopolysaccharide-induced acute lung injury. Crit Care. 2019;23:44.

[47] Malas MB, Naazie IN, Elsayed N, et al. Thromboembolism risk of COVID-19 is high and associated with a higher risk of mortality: A systematic review and meta-analysis. EClinicalMedicine. 2020;29:100639.

[48] Roberts LN, Whyte MB, Georgiou L, et al. Postdischarge venous thromboembolism following hospital admission with COVID-19. Blood. 2020;136:1347.

[49] Kanso M, Cardi T, Marzak H, et al. Delayed pulmonary embolism after COVID-19 pneumonia: a case report. Eur Hear J - Case Reports. 2020;4:1–4.

[50] Xiong Y, Liu Y, Cao L, et al. Transcriptomic characteristics of bronchoalveolar lavage fluid and peripheral blood mononuclear cells in COVID-19 patients. Emerg Microbes Infect. 2020;9:761–770.

[51] Cao D, Mikosz AM, Ringsby AJ, et al. MicroRNA-126-3p Inhibits Angiogenic Function of Human Lung Microvascular Endothelial Cells via LAT1 (L-Type Amino Acid Transporter 1)-Mediated mTOR (Mammalian Target of Rapamycin) Signaling. Arterioscler Thromb Vasc Biol. 2020;40:1195–1206.

[52] Katira BH, Giesinger RE, Engelberts D, et al. Adverse heart–lung interactions in ventilator-induced lung injury. Am J Respir Crit Care Med. 2017;196:1411–1421.

[53] Salamanna F, Veronesi F, Martini L, et al. Post-COVID-19 Syndrome: The Persistent Symptoms at the Post-viral Stage of the Disease. A Systematic Review of the Current Data. Front Med. 2021;0:392.

[54] Pinilla L, Benitez ID, González J, et al. Peripheral blood microRNAs and the COVID-19 patient: methodological considerations, technical challenges and practice points [Internet]. RNA Biol. Bellwether Publishing, Ltd.; 2021 [cited 2021 Jun 17]. p. 688–695.

Figure legends

Figure 1. Molecular mechanisms associated with pulmonary function in survivors of SARS-CoV-2-induced ARDS. A) Volcano plot representing the p-value versus the fold change for each microRNA after comparison of D_{LCO} tertiles. The red dot indicates significant differences. B) Prediction model based on Random Forest. On the left, the importance of the contribution of each microRNA to the model. On the right, the best combination of microRNAs selected by the algorithm to reduce the error. C) Correlation between microRNAs that composed the signature. D) Linear or nonlinear relationship between the levels of each microRNA that composed the signature and D_{LCO}. The expression levels are expressed as $\log_{10}$ ($2^{-\Delta Cq}$) for statistical purposes. E) Kyoto Encyclopedia of Genes and Genomes (KEGG) analysis (selected). F) Gene Ontology (GO) analysis (selected). The p-value denotes the significance of the molecular pathway or the biological process and the size of the points represents the number of genes involved. The false discovery rate adjusted p-value cutoff was 0.05.

Figure 2. Molecular mechanisms associated with radiologic features in survivors of SARS-CoV-2-induced ARDS. A) Volcano plot representing the p-value versus the fold change for each microRNA after comparison of TSS tertiles. The red dots indicate significant differences. B) Prediction model based on Random Forest. On the left, the importance of the contribution of each microRNA to the model. On the right, the best

combination of microRNAs selected by the algorithm to reduce the error. C) Correlation between microRNAs that composed the signature. D) Linear or nonlinear relationship between the levels of each microRNA that composed the signature and D_{LCO}. The expression levels are expressed as $\log_{10}$ ($2^{-\Delta Cq}$) for statistical purposes. E) Kyoto Encyclopedia of Genes and Genomes (KEGG) analysis (selected). F) Gene Ontology (GO) analysis (selected). The p-value denotes the significance of the molecular pathway or the biological process and the size of the points represents the number of genes implicated. The false discovery rate adjusted p-value cutoff was 0.05.

Figure 3. Molecular mechanisms associated with pulmonary function and/or radiologic features. A) Venn diagram displaying the shared and unique Kyoto Encyclopedia of Genes and Genomes (KEGG) pathways (selected). B) Venn diagram displaying the shared and unique Gene Ontology (GO) terms (selected). The size of each circle is proportional to the total number of molecular pathways or biological processes related to D_{LCO} and TSS. On the right, significant shared KEGG pathways and GO terms are reported for each diagram.

Identification of circulating microRNA profiles associated with pulmonary function and radiologic features in survivors of SARS-CoV-2-induced ARDS

María C. García-Hidalgo,[1] Jessica González,[1,2] Iván D. Benítez,[1,2] Paola Carmona,[1] Sally Santisteve,[1] Manel Pérez-Pons,[1,2] Anna Moncusí-Moix,[1,2] Clara Gort-Paniello,[1,2] Fátima Rodríguez-Jara,[1] Marta Molinero,[1] Thalia Belmonte,[1,2] Gerard Torres,[1,2] Gonzalo Labarca,[3,4] Estefania Nova-Lamperti,[3] Jesús Caballero,[5] Jesús F. Bermejo-Martin,[2,6] Adrián Ceccato,[2] Laia Fernández-Barat,[2,7] Ricard Ferrer,[2,8] Dario Garcia-Gasulla,[9] Rosario Menéndez,[2,10] Ana Motos,[2,7] Oscar Peñuelas,[2,11] Jordi Riera,[2,8] Antoni Torres,[2,7] Ferran Barbé,[1,2] David de Gonzalo-Calvo,[1,2,*]

on behalf of the CIBERESUCICOVID Project (COV20/00110, ISCIII).

[1] Translational Research in Respiratory Medicine, University Hospital Arnau de Vilanova and Santa Maria, IRBLleida, Lleida, Spain.

[2] CIBER of Respiratory Diseases (CIBERES), Institute of Health Carlos III, Madrid, Spain.

[3] Molecular and Translational Immunology Laboratory, Department of Clinical Biochemistry and Immunology, Faculty of Pharmacy, Universidad de Concepcion, Concepcion, Chile.

[4] Internal Medicine Unit, Complejo Asistencial Dr. Víctor Ríos Ruiz, Los Ángeles, Chile.

[5] Intensive Care Department, University Hospital Arnau de Vilanova, IRBLleida, Lleida, Spain. [6] Hospital Universitario Río Hortega de Valladolid, Valladolid, Spain; Instituto de Investigación Biomédica de Salamanca (IBSAL), Salamanca, Spain.

[7] Servei de Pneumologia, Hospital Clinic; Universitat de Barcelona; IDIBAPS, Barcelona, Spain.

[8] Intensive Care Department, Vall d'Hebron Hospital Universitari. SODIR Research Group, Vall d'Hebron Institut de Recerca (VHIR), Spain.

[9] Barcelona Supercomputing Center (BSC), Barcelona, Spain.

[10] Pulmonology Service, University and Polytechnic Hospital La Fe, Valencia, Spain.

[11] Hospital Universitario de Getafe, Madrid, Spain.

Correspondence to:

David de Gonzalo-Calvo, Ph.D.

Translational Research in Respiratory Medicine, University Hospital Arnau de Vilanova and Santa Maria, IRBLleida.

Avda. Alcalde Rovira Roure 80 · 25198 Lleida, Spain.

E-mail: dgonzalo@irblleida.cat

Tables

Table 1. Characteristics of the study population.

Sociodemographic characteristics		
N= 154		
Age (years)	61.0 [53.2;66.8]	154
Sex		154
Female	47 (30.5%)	
BMI (kg/m^2)	29.0 [26.1;33.3]	152
Smoking history		151
Former	79 (52.3%)	
Non-smoker	65 (43.0%)	
Current	7 (4.64%)	
Clinical characteristics		
Hypertension	76 (50.0%)	152
Type II Diabetes Mellitus	30 (19.7%)	152
Obesity	61 (40.1%)	152
Cardiovascular disease	11 (7.24%)	152
Previous Chronic Lung Disease	14 (9.21%)	152
Asthma	12 (7.89%)	152
Chronic kidney disease	3 (1.97%)	152
Chronic liver disease	7 (4.61%)	152
Baseline characteristics in hospital admission		
Oxygen saturation (%)	92.0 [89.0;94.0]	141
PaO_2/FiO_2	233 [155;286]	142
SaO_2/FiO_2	345 [180;438]	140
Hospital stay		
Worst PaO_2/FiO_2	134.0 [91.0;186.3]	154
ARDS classification		154
Mild (201-300 mmHg)	33 (21.4%)	
Moderate (101-200 mmHg)	70 (45.5%)	
Severe (≤100 mmHg)	51 (33.1%)	
Hospital stay (days)	18.0 [11.0;31.2]	152
ICU admission	127 (82.5%)	154
ICU stay (days)	11.0 [5.00;25.0]	125
High-flow nasal cannula	94 (61.0%)	154
Invasive mechanical ventilation (IMV)	64 (42.4%)	151
IMV duration (days)	17.0 [10.0;25.5]	63
Non-IMV	85 (56.7%)	150
Non-IMV duration (days)	3.00 [2.00;5.00]	84
Prone positioning	60 (40.0%)	150
Prone positioning duration (hours)	39.0 [23.0;72.0]	56
Antibiotics	122 (81.3%)	150
Hydroxychloroquine	68 (45.0%)	151
Tocilizumab	82 (53.9%)	152
Corticoids	129 (85.4%)	151

Remdesivir	29 (19.2%)	151
Interferon beta	20 (16.8%)	119
Lopinavir/ritonavir	65 (43.0%)	151
Corticoids at hospital discharge	36 (26.1%)	138
Post-COVID parameters		
D_{LCO}	66.2 [56.4;76.1]	154
<60	49 (31.8%)	
<80	77 (50.0%)	
≥80	28 (18.2%)	
TSS	5.00 [2.00;8.00]	151

Continuous variables are expressed as median [P_{25};P_{75}]. Categorical variables are expressed as n (%). ARDS: acute respiratory distress syndrome. BMI: body mass index. D_{LCO}: carbon monoxide diffusing capacity. FiO_2: fraction of inspired oxygen. ICU: intensive care unit. IMV: invasive mechanical ventilation. PaO_2: oxygen partial pressure. SaO_2: arterial oxygen saturation. TSS: total severity score.

Table 2. Characteristics of patients who entered in the inclusion criteria based on D_{LCO} tertiles.

	T1 [24.4, 60.1]	T2 (60.1, 72.3]	T3 (72.3, 100]	p-value	N
	N=51	N=50	N=53		
Sociodemographic characteristics					
Age (years)	64.0 [58.5;69.5]	56.5 [48.0;64.5]	59.0 [54.0;64.0]	0.026	154
Sex				0.175	154
Female	11 (21.6%)	18 (36.0%)	18 (34.0%)		
BMI (kg/m^2)	28.7 [26.2;32.4]	29.2 [25.5;34.2]	29.3 [26.5;33.2]	0.497	152
Smoking history				0.678	151
Former	29 (56.9%)	23 (47.9%)	27 (51.9%)		
Non-smoker	20 (39.2%)	22 (45.8%)	23 (44.2%)		
Current	2 (3.92%)	3 (6.25%)	2 (3.85%)		
Clinical characteristics					
Hypertension	29 (56.9%)	23 (46.9%)	24 (46.2%)	0.280	152
Type II Diabetes Mellitus	10 (19.6%)	9 (18.4%)	11 (21.2%)	0.843	152
Obesity	20 (39.2%)	22 (44.9%)	19 (36.5%)	0.779	152
Cardiovascular disease	7 (13.7%)	2 (4.08%)	2 (3.85%)	0.055	152
Chronic lung disease	6 (11.8%)	5 (10.2%)	3 (5.77%)	0.294	152
Asthma	2 (3.92%)	6 (12.2%)	4 (7.69%)	0.484	152
Chronic kidney disease	1 (1.96%)	0 (0.00%)	2 (3.85%)	0.489	152
Chronic liver disease	2 (3.92%)	2 (4.08%)	3 (5.77%)	0.655	152
Baseline characteristics in hospital admission					
Oxygen saturation (%)	91.5 [89.0;93.0]	93.0 [90.0;95.0]	91.0 [89.0;93.0]	0.998	141
PaO_2/FiO_2	236 [163;295]	238 [173;305]	227 [134;276]	0.300	142
SaO_2/FiO_2	413 [244;438]	358 [171;438]	275 [178;429]	0.093	140
Hospital stay					
Worst PaO_2/FiO_2	122.0 [90.5;188.0]	134.0 [95.5;175.0]	134.0 [80.0;188.0]	0.984	154
ARDS classification				0.918	154
Mild (201-300 mmHg)	11 (21.6%)	9 (18.0%)	13 (24.5%)		
Moderate (101-200 mmHg)	24 (47.1%)	25 (50.0%)	21 (39.6%)		
Severe (≤100 mmHg)	16 (31.4%)	16 (32.0%)	19 (35.8%)		
Hospital stay (days)	27.0 [15.5;44.5]	15.0 [10.0;31.0]	15.0 [10.0;23.8]	0.001	152
ICU admission	41 (80.4%)	43 (86.0%)	43 (81.1%)	0.928	154
ICU stay (days)	16.0 [7.25;33.8]	9.00 [5.00;21.0]	7.50 [5.00;18.2]	0.014	125
High flow nasal cannula	31 (60.8%)	32 (64.0%)	31 (58.5%)	0.261	154
IMV	27 (52.9%)	17 (35.4%)	20 (38.5%)	0.140	151
IMV duration (days)	18.0 [10.0;31.0]	18.0 [11.8;32.2]	13.5 [9.75;18.2]	0.077	63
Non-IMV	33 (64.7%)	22 (46.8%)	30 (57.7%)	0.480	150
Non-IMV duration (days)	3.00 [2.00;6.00]	3.00 [2.00;4.00]	2.50 [1.25;3.00]	0.037	84
Prone positioning	27 (52.9%)	17 (35.4%)	16 (31.4%)	0.027	150
Prone positioning duration (hours)	34.5 [15.8;57.8]	41.5 [21.8;85.5]	37.5 [26.8;62.8]	0.451	56

Antibiotics	39 (76.5%)	43 (89.6%)	40 (78.4%)	0.800	150
Hydroxychloroquine	22 (43.1%)	24 (49.0%)	22 (43.1%)	1.000	151
Tocilizumab	30 (58.8%)	27 (55.1%)	25 (48.1%)	0.275	152
Corticoids	44 (86.3%)	43 (89.6%)	42 (80.8%)	0.427	151
Remdesivir	10 (19.6%)	9 (18.4%)	10 (19.6%)	1.000	151
Interferon beta	7 (17.9%)	7 (17.9%)	6 (14.6%)	0.691	119
Lopinavir/ritonavir	22 (43.1%)	21 (42.9%)	22 (43.1%)	1.000	151
Corticoids at hospital discharge	14 (30.4%)	11 (23.4%)	11 (24.4%)	0.708	138
Post-COVID parameters					
D_{LCO}	51.5 [46.0;56.3]	66.0 [63.4;70.2]	80.4 [75.4;86.7]	<0.001	154
D_{LCO}				0.000	154
<60	49 (96.1%)	0 (0.00%)	0 (0.00%)		
<80	2 (3.92%)	50 (100%)	25 (47.2%)		
≥80	0 (0.00%)	0 (0.00%)	28 (52.8%)		
TSS score	9.00 [5.00;12.0]	4.50 [2.00;7.00]	3.50 [1.00;6.00]	<0.001	151

Continuous variables are expressed as median [P_{25};P_{75}]. Categorical variables are expressed as n (%). ARDS: acute respiratory distress syndrome. BMI: body mass index. D_{LCO}: carbon monoxide diffusing capacity. FiO_2: fraction of inspired oxygen. ICU: intensive care unit. IMV: invasive mechanical ventilation. PaO_2: oxygen partial pressure. SaO_2: arterial oxygen saturation. TSS: total severity score.

Table 3. Characteristics of patients who entered in the inclusion criteria based on TSS tertiles.

	T1 [0,3]	**T2 (3,7]**	**T3 (7,20]**	**p-value**	**N**
	N=56	N=53	N=42		
Sociodemographic characteristics					
Age (years)	56.0 [48.0;62.0]	62.0 [56.0;67.0]	66.0 [60.2;71.0]	<0.001	151
Sex				0.285	151
Male	37 (66.1%)	37 (69.8%)	32 (76.2%)		
Female	19 (33.9%)	16 (30.2%)	10 (23.8%)		
BMI (kg/m^2)	29.2 [26.5;34.7]	29.1 [25.6;32.9]	28.7 [27.0;32.7]	0.583	149
Smoking history				0.109	148
Former	28 (50.9%)	24 (47.1%)	26 (61.9%)		
Non-smoker	21 (38.2%)	27 (52.9%)	15 (35.7%)		
Current	6 (10.9%)	0 (0.00%)	1 (2.38%)		
Clinical characteristics					
Hypertension	21 (38.2%)	32 (61.5%)	22 (52.4%)	0.125	149
Type II Diabetes Mellitus	8 (14.5%)	13 (25.0%)	9 (21.4%)	0.358	149
Obesity	23 (41.8%)	22 (42.3%)	15 (35.7%)	0.566	149
Cardiovascular disease	3 (5.45%)	3 (5.77%)	5 (11.9%)	0.249	149
Chronic lung disease	5 (9.09%)	5 (9.62%)	4 (9.52%)	0.938	149
Asthma	7 (12.7%)	3 (5.77%)	2 (4.76%)	0.139	149
Chronic kidney disease	1 (1.82%)	0 (0.00%)	2 (4.76%)	0.361	149
Chronic liver disease	3 (5.45%)	1 (1.92%)	3 (7.14%)	0.769	149
Baseline characteristics in hospital admission					
Oxygen saturation (%)	92.0 [89.2;93.8]	92.0 [89.0;94.0]	91.5 [89.0;94.0]	0.675	139
PaO_2/FiO_2	220 [134;263]	248 [179;294]	229 [134;300]	0.413	139
SaO_2/FiO_2	325 [174;433]	410 [234;443]	332 [172;432]	0.482	138
Hospital stay					
Worst PaO_2/FiO_2	126.0 [87.5;175.0]	140.0 [118.0;176.0]	113.0 [85.2;206.0]	0.664	151
ARDS classification				0.463	151
Mild (201-300 mmHg)	11 (19.6%)	10 (18.9%)	12 (28.6%)		
Moderate (101-200 mmHg)	22 (39.3%)	32 (60.4%)	13 (31.0%)		
Severe (≤100 mmHg)	23 (41.1%)	11 (20.8%)	17 (40.5%)		
Hospital stay (days)	15.0 [10.0;24.5]	17.5 [10.8;31.2]	26.5 [17.0;45.8]	0.001	149
ICU admission	46 (82.1%)	43 (81.1%)	37 (88.1%)	0.465	151
ICU stay (days)	6.00 [3.00;12.8]	6.00 [3.75;17.5]	15.0 [5.50;32.5]	0.003	148
High flow nasal cannula	31 (55.3%)	38 (71.7%)	24 (57.2%)	0.849	151
IMV	17 (30.9%)	23 (45.1%)	24 (57.1%)	0.010	148
IMV duration (days)	0.00 [0.00;5.00]	0.00 [0.00;13.0]	8.00 [0.00;25.0]	0.002	147
Non-IMV	29 (53.7%)	27 (52.9%)	28 (66.7%)	0.226	147
Non-IMV duration (days)	1.00 [0.00;3.00]	1.00 [0.00;3.00]	2.50 [0.00;4.75]	0.061	146
Prone positioning	16 (29.6%)	19 (37.3%)	25 (59.5%)	0.004	147

Prone positioning duration (hours)	0.00 [0.00;5.00]	0.00 [0.00;19.5]	17.5 [0.00;47.5]	<0.001	143
Antibiotics	46 (85.2%)	40 (78.4%)	36 (85.7%)	0.991	147
Hydroxychloroquine	31 (57.4%)	19 (36.5%)	18 (42.9%)	0.125	148
Tocilizumab	26 (47.3%)	31 (59.6%)	23 (54.8%)	0.417	149
Corticoids	44 (80.0%)	46 (90.2%)	36 (85.7%)	0.380	148
Remdesivir	7 (13.0%)	10 (19.2%)	10 (23.8%)	0.170	148
Interferon beta	5 (12.5%)	6 (14.6%)	9 (24.3%)	0.172	118
Lopinavir/ritonavir	28 (51.9%)	19 (36.5%)	18 (42.9%)	0.330	148
Corticoids at discharge	9 (18.8%)	16 (32.7%)	10 (26.3%)	0.295	135
Post-COVID parameters					
D_{LCO}	71.3 [65.0;81.6]	70.0 [56.6;78.1]	54.7 [48.1;62.5]	<0.001	151
D_{LCO}				<0.001	151
<60	7 (12.5%)	14 (26.4%)	26 (61.9%)		
<80	32 (57.1%)	29 (54.7%)	15 (35.7%)		
≥80	17 (30.4%)	10 (18.9%)	1 (2.38%)		
TSS score	2.00 [0.00;2.25]	5.00 [5.00;7.00]	11.0 [10.0;13.0]	<0.001	151

Continuous variables are expressed as median [P_{25};P_{75}]. Categorical variables are expressed as n (%). ARDS: acute respiratory distress syndrome. BMI: body mass index. D_{LCO}: carbon monoxide diffusing capacity. FiO_2: fraction of inspired oxygen. ICU: intensive care unit. IMV: invasive mechanical ventilation. PaO_2: oxygen partial pressure. SaO_2: arterial oxygen saturation. TSS: total severity score.

Supplemental online material

Identification of circulating microRNA profiles associated with pulmonary function and radiologic features in survivors of SARS-CoV-2-induced ARDS

María C. García-Hidalgo,[1] Jessica González,[1,2] Iván D. Benítez,[1,2] Paola Carmona,[1] Sally Santisteve,[1] Manel Pérez-Pons,[1,2] Anna Moncusí-Moix,[1,2] Clara Gort-Paniello,[1,2] Fátima Rodríguez-Jara,[1] Marta Molinero,[1] Thalia Belmonte,[1,2] Gerard Torres,[1,2] Gonzalo Labarca,[3,4] Estefania Nova-Lamperti,[3] Jesús Caballero,[5] Jesús F. Bermejo-Martin,[2,6] Adrián Ceccato,[2] Laia Fernández-Barat,[2,7] Ricard Ferrer,[2,8] Dario Garcia-Gasulla,[9] Rosario Menéndez,[2,10] Ana Motos,[2,7] Oscar Peñuelas,[2,11] Jordi Riera,[2,8] Antoni Torres,[2,7] Ferran Barbé,[1,2] David de Gonzalo-Calvo,[1,2,*]

on behalf of the CIBERESUCICOVID Project (COV20/00110, ISCIII).

[1] Translational Research in Respiratory Medicine, University Hospital Arnau de Vilanova and Santa Maria, IRBLleida, Lleida, Spain.

[2] CIBER of Respiratory Diseases (CIBERES), Institute of Health Carlos III, Madrid, Spain.

[3] Molecular and Translational Immunology Laboratory, Department of Clinical Biochemistry and Immunology, Faculty of Pharmacy, Universidad de Concepcion, Concepcion, Chile.

[4] Internal Medicine Unit, Complejo Asistencial Dr. Víctor Ríos Ruiz, Los Ángeles, Chile.

[5] Intensive Care Department, University Hospital Arnau de Vilanova, IRBLleida, Lleida, Spain. [6] Hospital Universitario Río Hortega de Valladolid, Valladolid, Spain; Instituto de Investigación Biomédica de Salamanca (IBSAL), Salamanca, Spain.

[7] Servei de Pneumologia, Hospital Clinic; Universitat de Barcelona; IDIBAPS, Barcelona, Spain.

[8] Intensive Care Department, Vall d'Hebron Hospital Universitari. SODIR Research Group, Vall d'Hebron Institut de Recerca (VHIR), Spain.

[9] Barcelona Supercomputing Center (BSC), Barcelona, Spain.

[10] Pulmonology Service, University and Polytechnic Hospital La Fe, Valencia, Spain.

[11] Hospital Universitario de Getafe, Madrid, Spain.

Correspondence to:

David de Gonzalo-Calvo, Ph.D.

Translational Research in Respiratory Medicine, University Hospital Arnau de Vilanova and Santa Maria, IRBLleida.

Avda Alcalde Rovira Roure 80 · 25198 Lleida, Spain.

E-mail: dgonzalo@irblleida.cat

Supplemental Figures

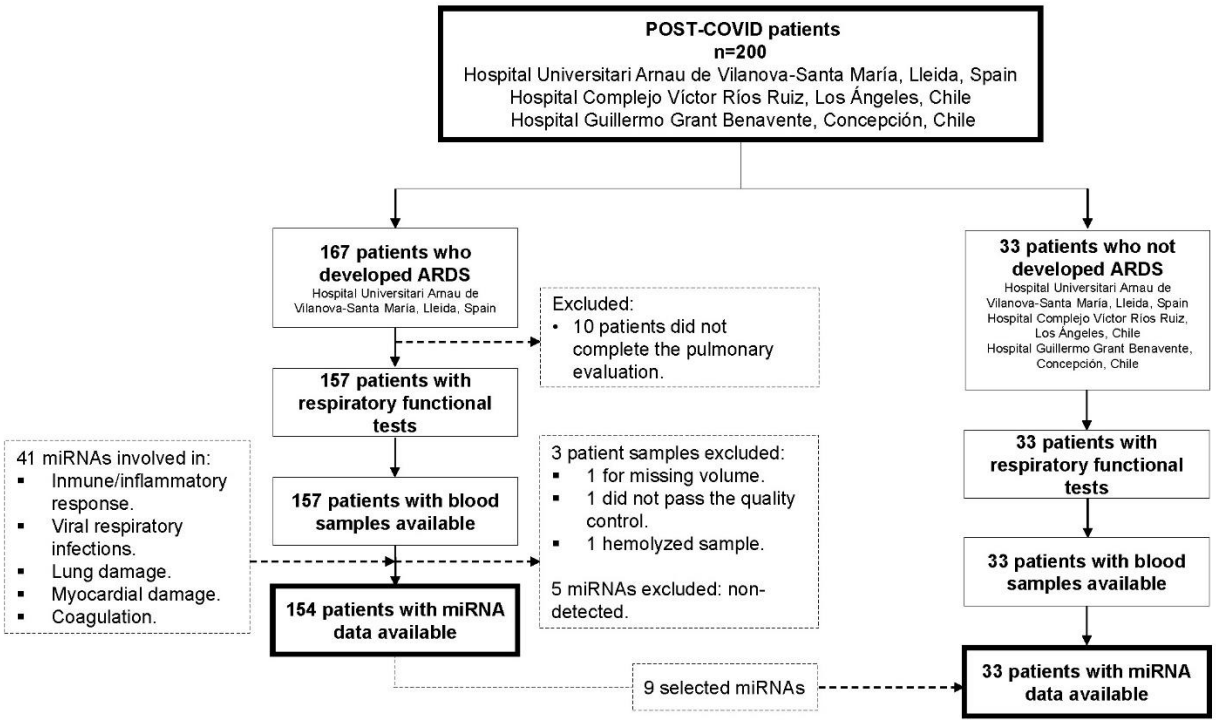

Supplemental Figure S1. Study flowchart. A total of 167 patients infected by SARS-CoV-2 in the first and second waves who developed ARDS as a consequence attended follow-up. After excluding patients who did not complete respiratory functional tests, 157 samples were available for microRNA quantification. Three samples were not included in the final analyses due to missing volume, hemolysis and high variability in quality control. Additionally, we did not include five nondetected microRNAs (miR-34b-5p, miR-34c-5p, miR-124-3p, miR-208a-3p and miR-208b-3p). A control cohort (n=33), composed by patients positive for SARS-CoV-2 but who did not develop ARDS was included to analyze the specificity of the associations between circulating miRNA profiles and pulmonary function and radiologic features in survivors of SARS-CoV-2-induced ARDS.

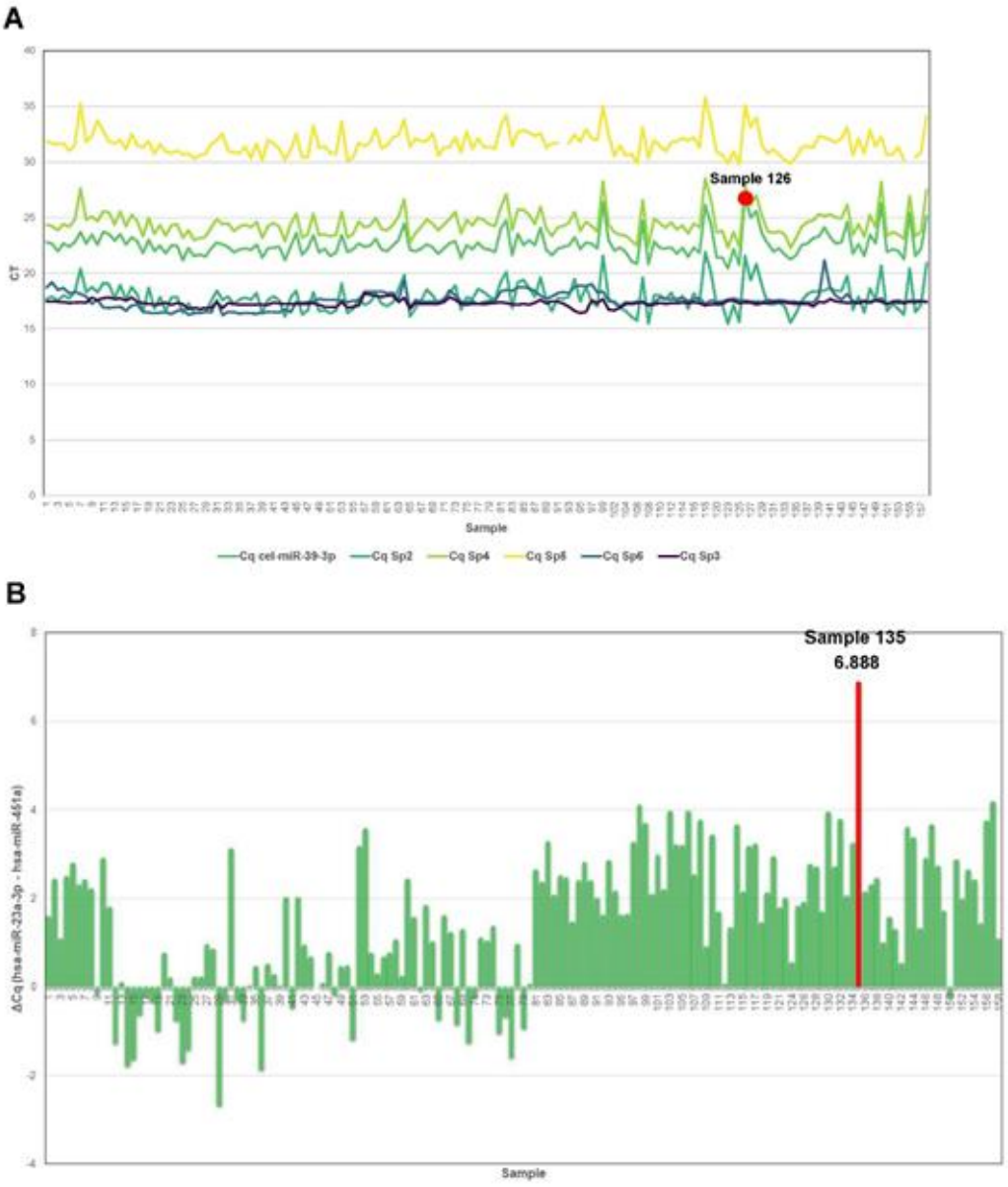

Supplemental Figure S2. Quality control. A) Spike-in levels. B) Hemolysis test.

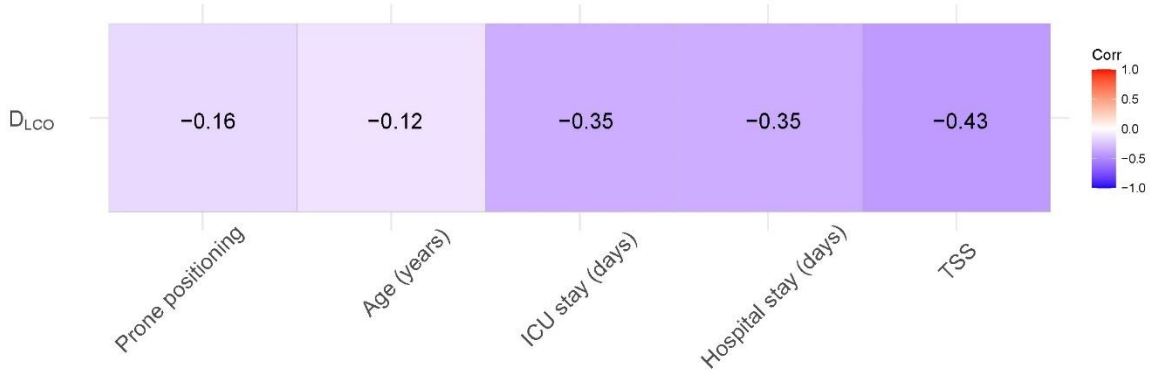

Supplemental Figure S3. Correlation between D_{LCO} levels and demographic and clinical variables. Point-biserial correlation was used to estimate the correlation between dichotomous and continuous variables, represented as r_{pb} values, and Spearman's test was used to estimate the correlation between continuous variables, represented as rho values.

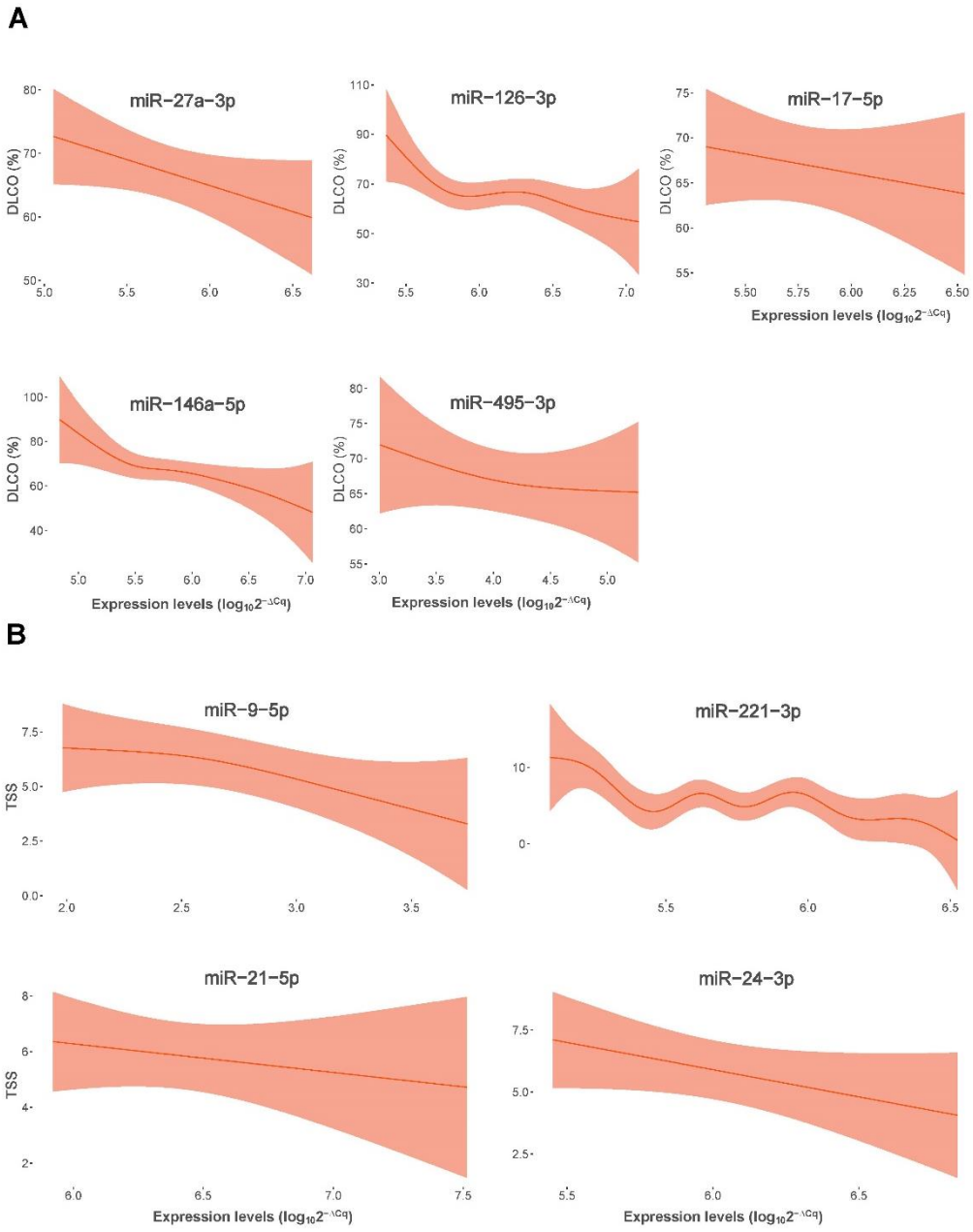

Supplemental Figure S4. Age, sex, previous chronic pulmonary disease, smoking history and the use of corticoids after hospital discharge showed no significant impact on the association between microRNA levels and pulmonary function or radiologic features. A) Representation of the linear or nonlinear relationship between the value of DLCO and the expression levels of each of the microRNAs of the signature adjusted by age, sex, previous chronic pulmonary disease, smoking history and the use of corticoids after

hospital discharge. B) Representation of the linear or nonlinear relationship between the value of TSS and the expression levels of each of the microRNAs of the signature adjusted by age, sex, previous chronic pulmonary disease, smoking history and the use of corticoids after hospital discharge. microRNA expression levels are expressed as $\log_{10}(2^{-\Delta Cq})$ for statistical purposes.

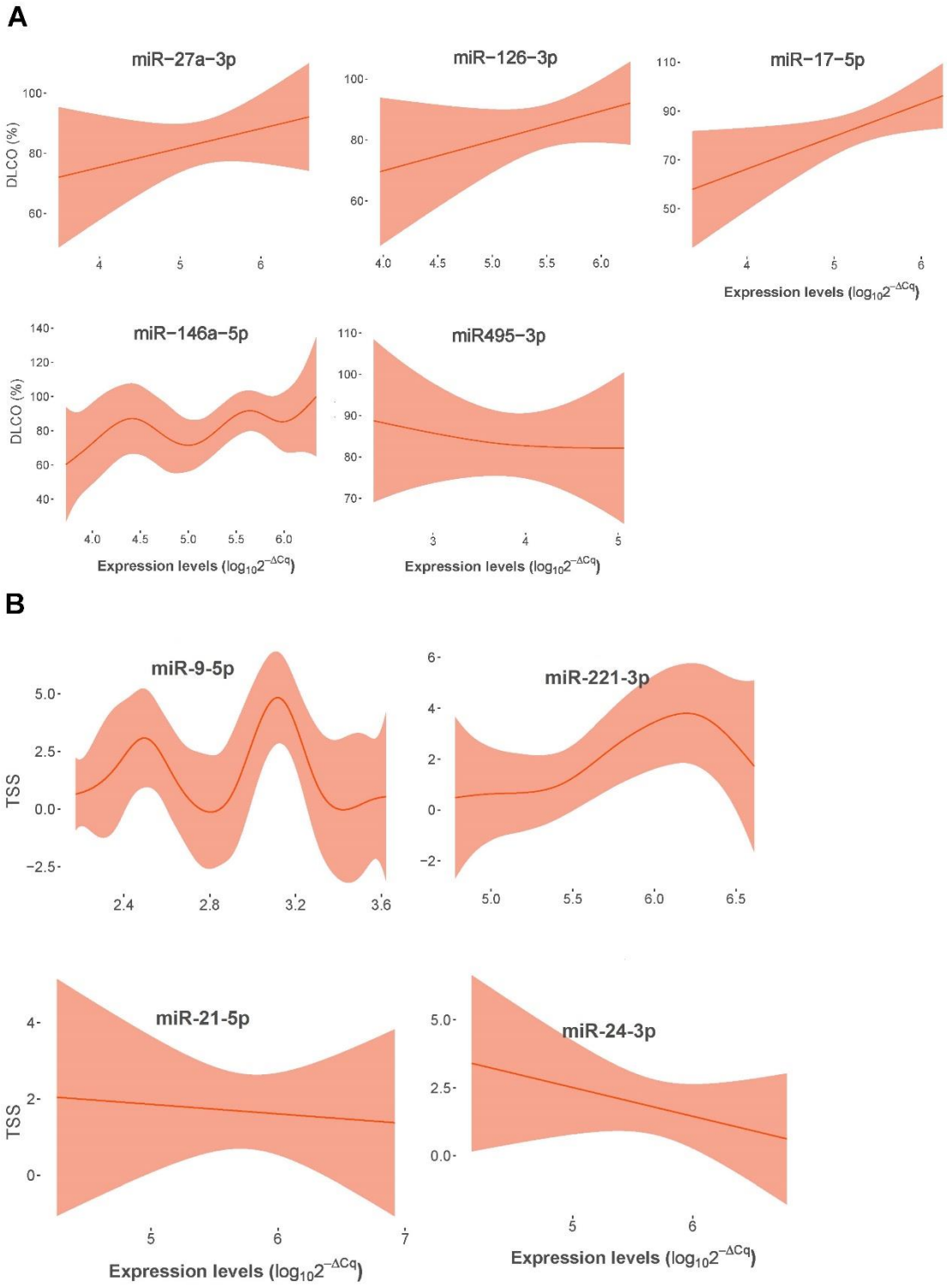

Supplemental Figure S5. Linear or nonlinear relationship between the levels of each microRNA that composed the signatures and diffusion capacity and radiological features, respectively, in patients positive for SARS-CoV-2 who did developed ARDS. A) GAM

modeling for D_{LCO} (Y axis) and expression levels (expressed as $\log_{10} 2^{-\Delta Cq}$) (X axis). B) GAM modeling for TSS (Y axis) and expression levels (expressed as $\log_{10} 2^{-\Delta Cq}$) (X axis).

Supplemental Figure S6. Correlation between individual miRNAs in both signatures and clinical variables related to the severity of the acute phase. Spearman's test was used to calculate the correlation between the variables, represented as rho values.

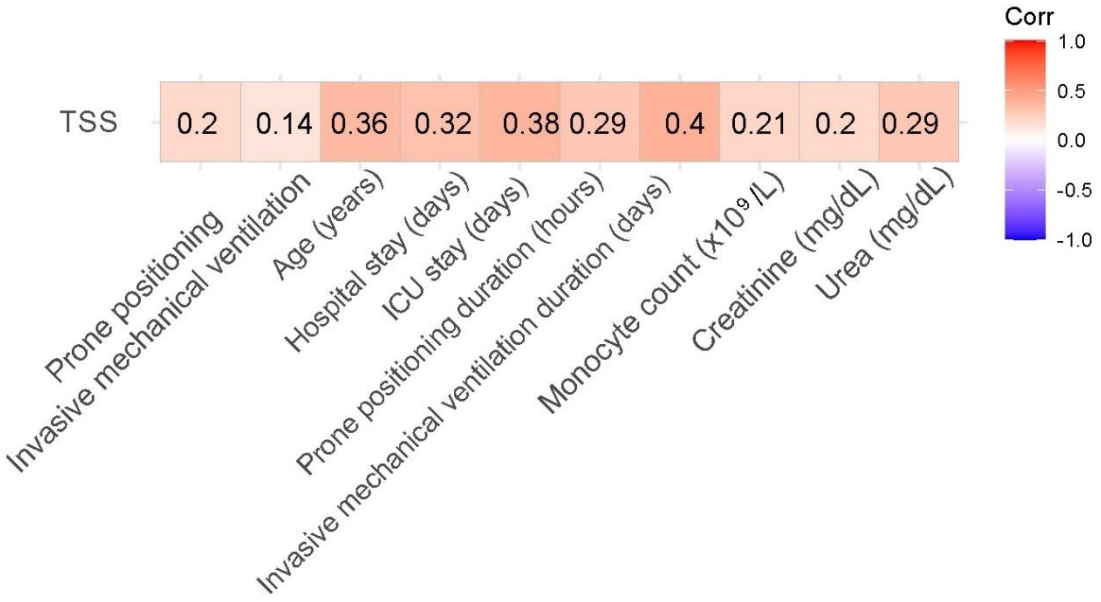

Supplemental Figure S7. Correlation between TSS levels and demographic and clinical variables. Point-biserial correlation was used to estimate the correlation between dichotomous and continuous variables, represented as r_{pb} values, and Spearman's test was used to estimate the correlation between continuous variables, represented as rho values.

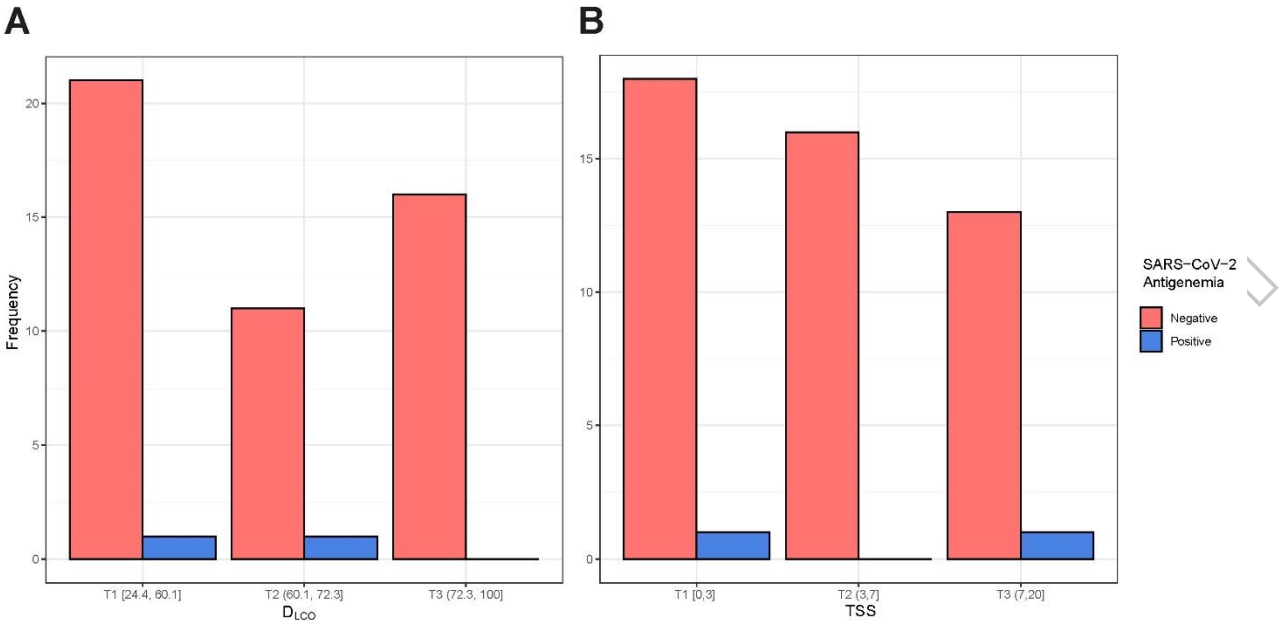

Supplemental Figure S8. SARS-CoV-2 antigenemia in plasma. A) SARS-CoV-2 antigen detection in plasma samples according to D_{LCO} tertiles. B) SARS-CoV-2 antigen detection in plasma samples according to TSS tertiles.

Supplemental Tables

Supplemental Table S1. Panel of miRNAs analyzed in the study population.

microRNA ID	miRBase Accession Number	MiRCury Assay	Target sequence
hsa-miR-1-3p	MIMAT0000416	YP00204344	UGGAAUGUAAAGAAGUAUGUAU
hsa-miR-9-5p	MIMAT0000441	YP00204513	UCUUUGGUUAUCUAGCUGUAUGA
hsa-miR-16-5p	MIMAT0000069	YP00205702	UAGCAGCACGUAAAUAUUGGCG
hsa-miR-17-5p	MIMAT0000070	YP02119304	CAAAGUGCUUACAGUGCAGGUAG
hsa-miR-21-5p	MIMAT0000076	YP00204230	UAGCUUAUCAGACUGAUGUUGA
hsa-miR-24-3p	MIMAT0000080	YP00204260	UGGCUCAGUUCAGCAGGAACAG
hsa-miR-27a-3p	MIMAT0000084	YP00206038	UUCACAGUGGCUAAGUUCCGC
hsa-miR-27b-3p	MIMAT0000419	YP00205915	UUCACAGUGGCUAAGUUCUGC
hsa-miR-34a-5p	MIMAT0000255	YP00204486	UGGCAGUGUCUUAGCUGGUUGU
hsa-miR-34b-5p	MIMAT0000685	YP00204424	UAGGCAGUGUCAUUAGCUGAUUG
hsa-miR-34c-5p	MIMAT0000686	YP00205659	AGGCAGUGUAGUUAGCUGAUUGC
hsa-miR-92a-3p	MIMAT0000092	YP00204258	UAUUGCACUUGUCCCGGCCUGU
hsa-miR-93-5p	MIMAT0000093	YP00204715	CAAAGUGCUGUUCGUGCAGGUAG
hsa-miR-98-5p	MIMAT0000096	YP00204640	UGAGGUAGUAAGUUGUAUUGUU
hsa-miR-122-5p	MIMAT0000421	YP00205664	UGGAGUGUGACAAUGGUGUUUG
hsa-miR-124-3p	MIMAT0000422	YP00206026	UAAGGCACGCGGUGAAUGCC
hsa-miR-125a-5p	MIMAT0000443	YP00204339	UCCCUGAGACCCUUUAACCUGUGA
hsa-miR-125b-5p	MIMAT0000423	YP00205713	UCCCUGAGACCCUAACUUGUGA
hsa-miR-126-3p	MIMAT0000445	YP00204227	UCGUACCGUGAGUAAUAAUGCG
hsa-miR-132-3p	MIMAT0000426	YP00206035	UAACAGUCUACAGCCAUGGUCG
hsa-miR-133a-3p	MIMAT0000427	YP00204788	UUUGGUCCCCUUCAACCAGCUG
hsa-miR-146a-5p	MIMAT0000449	YP00204688	UGAGAACUGAAUUCCAUGGGUU
hsa-miR-148a-3p	MIMAT0000243	YP00205867	UCAGUGCACUACAGAACUUUGU
hsa-miR-150-5p	MIMAT0000451	YP00204660	UCUCCCAACCCUUGUACCAGUG
hsa-miR-155-5p	MIMAT0000646	YP00204308	UUAAUGCUAAUCGUGAUAGGGGU
hsa-miR-181a-5p	MIMAT0000256	YP00206081	AACAUUCAACGCUGUCGGUGAGU
hsa-miR-192-5p	MIMAT0000222	YP00204099	CUGACCUAUGAAUUGACAGCC
hsa-miR-199a-5p	MIMAT0000231	YP00204494	CCCAGUGUUCAGACUACCUGUUC
hsa-miR-208a-3p	MIMAT0026474	YP00205619	AUAAGACGAGCAAAAAGCUUGU
hsa-miR-208b-3p	MIMAT0026722	YP00204636	AUAAGACGAACAAAAGGUUUGU
hsa-miR-214-3p	MIMAT0000271	YP00204510	ACAGCAGGCACAGACAGGCAGU
hsa-miR-221-3p	MIMAT0000278	YP00204532	AGCUACAUUGUCUGCUGGGUUUC

hsa-miR-222-3p	MIMAT0000279	YP00204551	AGCUACAUCUGGCUACUGGGU
hsa-miR-223-3p	MIMAT0000280	YP00205986	UGUCAGUUUGUCAAAUACCCCA
hsa-miR-323a-3p	MIMAT0000755	YP00204278	CACAUUACACGGUCGACCUCU
hsa-miR-451a	MIMAT0001631	YP02119305	AAACCGUUACCAUUACUGAGUU
hsa-miR-486-5p	MIMAT0002177	YP00204001	UCCUGUACUGAGCUGCCCCGAG
hsa-miR-491-5p	MIMAT0002807	YP00204695	AGUGGGGAACCCUUCCAUGAGG
hsa-miR-495-3p	MIMAT0002817	YP00206015	AAACAAACAUGGUGCACUUCUU
hsa-miR-499a-5p	MIMAT0002870	YP00205935	UUAAGACUUGCAGUGAUGUUU
hsa-miR-574-5p	MIMAT0004795	YP02116206	UGAGUGUGUGUGUGUGAGUGUGU

Supplemental Table S2. Characteristics of non-ARDS patients attended to Post-COVID evaluation.

	N=33	N
Sociodemographic characteristics		
Age (years), median [P_{25};P_{75}]	48.0 [37.0;61.0]	33
Sex, n(%):		33
Female	17 (51.5%)	
Male	16 (48.5%)	
Hospital stay		
Hospital admission	18 (54.5%)	33
Post-COVID parameters		
D_{LCO}, median [P_{25};P_{75}]	86.0 [67.3;94.0]	33
<60, n (%)	3 (9.09%)	
<80, n (%)	19 (57.6%)	
>=80, n (%)	11 (33.3%)	
TSS score, median [P_{25};P_{75}]	0.00 [0.00;2.00]	33

Continuous variables are expressed as median [P_{25};P_{75}]. Categorical variables are expressed as n (%). D_{LCO}: carbon monoxide diffusing capacity. TSS: total severity score.

Supplemental Table S3. KEGG analysis for the miRNA signature associated with D_{LCO}.

KEGG pathway	p-value	Number of Genes
Viral carcinogenesis	3.76×10^{-12}	87
Proteoglycans in cancer	4.03×10^{-11}	84
ECM-receptor interaction	6.96×10^{-11}	30
Prion diseases	4.34×10^{-9}	11
Chronic myeloid leukemia	6.78×10^{-9}	45
Hepatitis B	6.78×10^{-9}	71
Glioma	1.34×10^{-8}	36
Bacterial invasion of epithelial cells	2.04×10^{-8}	46
TGF-beta signaling pathway	2.75×10^{-8}	42
AMPK signaling pathway	4.14×10^{-8}	66
Hippo signaling pathway	4.17×10^{-8}	62
Pancreatic cancer	1.72×10^{-7}	37
Neurotrophin signaling pathway	5.26×10^{-7}	62
Fatty acid biosynthesis	6.11×10^{-7}	4
Thyroid hormone signaling pathway	8.40×10^{-7}	58
Renal cell carcinoma	1.00×10^{-6}	39
FoxO signaling pathway	1.05×10^{-6}	67
Pathways in cancer	8.14×10^{-6}	149
Prostate cancer	8.14×10^{-6}	48
Focal adhesion	1.05×10^{-5}	91
Prolactin signaling pathway	1.22×10^{-5}	37
Sphingolipid signaling pathway	1.40×10^{-5}	52
mTOR signaling pathway	1.94×10^{-5}	35
Small cell lung cancer	1.94×10^{-5}	45
Estrogen signaling pathway	2.20×10^{-5}	45
Non-small cell lung cancer	2.43×10^{-5}	29
Signaling pathways regulating pluripotency of stem cells	4.82×10^{-5}	59
Colorectal cancer	8.49×10^{-5}	34
Cell cycle	9.35×10^{-5}	55
Oocyte meiosis	9.75×10^{-5}	50
Endometrial cancer	1.00×10^{-4}	29
Progesterone-mediated oocyte maturation	1.25×10^{-4}	45
Central carbon metabolism in cancer	6.28×10^{-4}	31
Adherens junction	7.02×10^{-4}	35
mRNA surveillance pathway	7.02×10^{-4}	43
Insulin signaling pathway	7.53×10^{-4}	61
Thyroid cancer	1.07×10^{-3}	16
ErbB signaling pathway	1.42×10^{-3}	42
Transcriptional misregulation in cancer	1.57×10^{-3}	66
Bladder cancer	1.59×10^{-3}	23
Toxoplasmosis	1.59×10^{-3}	51

Ubiquitin mediated proteolysis	1.62×10^{-3}	59
HIF-1 signaling pathway	1.87×10^{-3}	48
Adrenergic signaling in cardiomyocytes	2.09×10^{-3}	52
PI3K-Akt signaling pathway	2.21×10^{-3}	119
Shigellosis	2.49×10^{-3}	30
Lysine degradation	2.65×10^{-3}	18
Melanoma	3.49×10^{-3}	31
Hepatitis C	3.87×10^{-3}	54
Protein processing in endoplasmic reticulum	4.21×10^{-3}	65
Mucin type O-Glycan biosynthesis	5.99×10^{-3}	12
HTLV-I infection	6.25×10^{-3}	95
Axon guidance	6.43×10^{-3}	48
p53 signaling pathway	6.55×10^{-3}	32
Leukocyte transendothelial migration	8.28×10^{-3}	44
TNF signaling pathway	9.05×10^{-3}	46
Acute myeloid leukemia	1.48×10^{-2}	27
Chagas disease (American trypanosomiasis)	1.58×10^{-2}	43
Epithelial cell signaling in Helicobacter pylori infection	3.22×10^{-2}	29
Choline metabolism in cancer	3.99×10^{-2}	41
Platelet activation	4.64×10^{-2}	45

Supplemental Table S4. GO analysis for the miRNA signature associated with D_{LCO}.

GO category	p-value	Number of Genes
Cellular nitrogen compound metabolic process	3.03 X 10^{-157}	1325
Biosynthetic process	1.60 X 10^{-111}	1106
Cellular protein modification process	1.31 X 10^{-97}	724
Gene expression	2.79 X 10^{-92}	261
Symbiosis. encompassing mutualism through parasitism	1.82 X 10^{-69}	224
Viral process	1.90 X 10^{-62}	197
Biological process	3.71 X 10-^{53}	3488
Response to stress	3.16 X 10^{-45}	606
Catabolic process	3.38 X 10^{-45}	520
Neurotrophin trk receptor signaling pathway	1.42 X 10^{-40}	108
Mitotic cell cycle	1.71 X 10^{-39}	148
Cellular protein metabolic process	1.50 X 10^{-37}	159
Membrane organization	3.30 X 10^{-33}	194
Small molecule metabolic process	5.96 X 10^{-32}	545
Cellular component assembly	5.73 X 10^{-30}	347
Blood coagulation	1.72 X 10^{-28}	147
Nucleobase-containing compound catabolic process	2.07 X 10^{-28}	255
Cell death	6.37 X 10^{-28}	266
Macromolecular complex assembly	3.36 X 10^{-26}	247
Fc-epsilon receptor signaling pathway	4.11 X 10^{-25}	65
Transcription. DNA-templated	1.12 X 10^{-20}	610
Trif-dependent toll-like receptor signaling pathway	2.13 X 10^{-19}	38
Toll-like receptor 10 signaling pathway	2.82 X 10^{-19}	35
Toll-like receptor tlr1:tlr2 signaling pathway	4.50 X 10^{-19}	36
Toll-like receptor tlr6:tlr2 signaling pathway	4.50 X 10^{-19}	36
mRNA metabolic process	1.64 X 10^{-18}	74
Toll-like receptor 9 signaling pathway	4.05 X 10^{-18}	38
Protein complex assembly	4.05 X 10^{-18}	205
Myd88-independent toll-like receptor signaling pathway	2.71 X 10^{-17}	38
Immune system process	2.73 X 10^{-17}	377
Epidermal growth factor receptor signaling pathway	6.26 X 10^{-17}	75
Toll-like receptor 5 signaling pathway	6.26 X 10^{-17}	35
Stress-activated mapk cascade	1.68 X 10^{-16}	33
RNA metabolic process	6.92 X 10^{-16}	79
Toll-like receptor 3 signaling pathway	7.08 X 10^{-16}	39
DNA metabolic process	2.25 X 10^{-15}	201
Fc-gamma receptor signaling pathway involved in phagocytosis	2.25 X 10^{-15}	34
Chromatin organization	6.33 X 10^{-15}	55
Post-translational protein modification	6.80 X 10^{-15}	56
Innate immune response	2.63 X 10^{-14}	190
Transcription initiation from RNA polymerase ii promoter	4.06 X 10^{-14}	78

Toll-like receptor 2 signaling pathway	5.17×10^{-14}	36
Activation of signaling protein activity involved in unfolded protein response	9.37×10^{-14}	32
Toll-like receptor 4 signaling pathway	2.40×10^{-13}	41
Toll-like receptor signaling pathway	4.58×10^{-13}	45
Fibroblast growth factor receptor signaling pathway	1.35 X 10-^{12}	66
Platelet activation	2.17×10^{-12}	64
G2/m transition of mitotic cell cycle	2.17×10^{-12}	56
Insulin receptor signaling pathway	3.77×10^{-12}	63
Transforming growth factor beta receptor signaling pathway	8.84×10^{-11}	69
Myd88-dependent toll-like receptor signaling pathway	1.11×10^{-10}	38
Cellular lipid metabolic process	2.00×10^{-10}	46
Cytoskeleton organization	7.74×10^{-10}	170
Phosphatidylinositol-mediated signaling	8.98×10^{-10}	48
Intrinsic apoptotic signaling pathway	1.92×10^{-8}	30
Cell junction organization	2.14×10^{-8}	49
Cellular component disassembly involved in execution phase of apoptosis	3.35×10^{-8}	20
Vesicle-mediated transport	5.27×10^{-8}	236
Protein n-linked glycosylation via asparagine	8.49×10^{-8}	34
Extracellular matrix disassembly	1.73×10^{-7}	35
Platelet degranulation	3.06×10^{-7}	26
Cell cycle	3.42×10^{-7}	222
Apoptotic signaling pathway	3.58×10^{-7}	44
Positive regulation of protein insertion into mitochondrial membrane involved in apoptotic signaling pathway	3.58×10^{-7}	16
mRNA processing	3.90×10^{-7}	138
Termination of RNA polymerase II transcription	3.92×10^{-7}	20
Viral life cycle	7.23×10^{-7}	33
Mitotic nuclear envelope disassembly	1.29×10^{-6}	16
Nucleocytoplasmic transport	1.31×10^{-6}	94
mRNA 3'-end processing	2.11×10^{-6}	18
Cell proliferation	2.88×10^{-6}	156
Transcription from RNA polymerase II promoter	3.21×10^{-6}	154
RNA splicing	4.37×10^{-6}	88
Axon guidance	7.56×10^{-6}	112
Nuclear-transcribed mRNA catabolic process. deadenylation-dependent decay	7.71×10^{-6}	23
Endoplasmic reticulum unfolded protein response	1.01×10^{-5}	42
Extracellular matrix organization	1.08×10^{-5}	90
Negative regulation of transcription from RNA polymerase ii promoter	1.08×10^{-5}	247
Type I interferon signaling pathway	1.11×10^{-5}	26
Jak-stat cascade involved in growth hormone signaling pathway	2.19×10^{-5}	13
Cell cycle arrest	2.29×10^{-5}	56
Cell junction assembly	2.36×10^{-5}	21
Nucleotide-binding domain. leucine rich repeat containing receptor signaling pathway	3.51×10^{-5}	18
Protein targeting	4.40×10^{-5}	72
Hexose transport	4.69×10^{-5}	15
Antigen processing and presentation of exogenous peptide antigen via mhc class ii	5.53×10^{-5}	35

Regulation of transcription from RNA polymerase II promoter in response to hypoxia	5.84×10^{-5}	14
G1/S transition of mitotic cell cycle	6.59×10^{-5}	50
Cellular component movement	6.69×10^{-5}	33
Chromatin modification	1.08×10^{-4}	56
Phosphatidylinositol biosynthetic process	1.08×10^{-4}	22
Generation of precursor metabolites and energy	1.31×10^{-4}	74
Cytokine-mediated signaling pathway	1.72×10^{-4}	76
Leukocyte migration	1.78×10^{-4}	32
Regulation of glucose transport	1.79×10^{-4}	13
Negative regulation of cell proliferation	1.81×10^{-4}	142
Nuclear-transcribed mRNA catabolic process. nonsense-mediated decay	2.54×10^{-4}	37
Positive regulation of type I interferon production	2.60×10^{-4}	21
Positive regulation of apoptotic process	5.29×10^{-4}	113
Nucleotide-binding oligomerization domain containing signaling pathway	5.41×10^{-4}	12
Positive regulation of transcription. DNA-templated	7.04×10^{-4}	207
Post-Golgi vesicle-mediated transport	7.79×10^{-4}	17
Regulation of ubiquitin-protein ligase activity involved in mitotic cell cycle	8.84×10^{-4}	20
Cell motility	9.25×10^{-4}	118
Phospholipid metabolic process	9.63×10^{-4}	41
Notch signaling pathway	9.85×10^{-4}	54
Protein polyubiquitination	1.17×10^{-3}	45
mRNA splicing. via spliceosome	1.29×10^{-3}	63
Protein maturation	1.41×10^{-3}	49
Anatomical structure morphogenesis	1.79×10^{-3}	29
Glycosaminoglycan metabolic process	1.94×10^{-3}	25
Protein ubiquitination	1.94×10^{-3}	130
Viral transcription	3.04×10^{-3}	20
Ribonucleoprotein complex assembly	3.04×10^{-3}	37
In utero embryonic development	3.16×10^{-3}	85
Vitamin metabolic process	3.47×10^{-3}	19
Ras protein signal transduction	3.96×10^{-3}	31
Nuclear-transcribed mRNA poly(A) tail shortening	4.20×10^{-3}	14
Srp-dependent cotranslational protein targeting to membrane	4.36×10^{-3}	30
Cellular response to hypoxia	4.59×10^{-3}	42
Positive regulation of ubiquitin-protein ligase activity involved in mitotic cell cycle	5.13×10^{-3}	18
Positive regulation of viral transcription	5.44×10^{-3}	15
Apoptotic process	5.44×10^{-3}	195
Regulation of small GTPase mediated signal transduction	5.44×10^{-3}	50
Transcription elongation from RNA polymerase II promoter	5.44×10^{-3}	22
Inositol phosphate metabolic process	5.94×10^{-3}	13
Positive regulation of muscle cell differentiation	5.94×10^{-3}	12
Regulation of transcription involved in g1/s transition of mitotic cell cycle	5.94×10^{-3}	12
O-glycan processing	6.07×10^{-3}	15
Water-soluble vitamin metabolic process	6.37×10^{-3}	17
Negative regulation of transforming growth factor beta receptor signaling pathway	7.67×10^{-3}	31

Energy reserve metabolic process	1.10×10^{-2}	23
Translational termination	1.10×10^{-2}	23
Nitric oxide metabolic process	1.11×10^{-2}	9
Cofactor metabolic process	1.12×10^{-2}	52
Negative regulation of apoptotic process	1.24×10^{-2}	159
Signal transduction	1.33×10^{-2}	989
Cellular response to ionizing radiation	1.46×10^{-2}	18
Negative regulation of transcription. DNA-templated	1.57×10^{-2}	174
Glycerophospholipid biosynthetic process	1.72×10^{-2}	20
Regulation of defense response to virus by virus	2.26×10^{-2}	9
Response to virus	2.47×10^{-2}	45
Androgen receptor signaling pathway	2.51×10^{-2}	18
Long-chain fatty-acyl-coa biosynthetic process	2.57×10^{-2}	7
Regulation of nitric-oxide synthase activity	2.77×10^{-2}	9
mRNA export from nucleus	2.96×10^{-2}	24
Transport	3.05×10^{-2}	757
Muscle cell differentiation	3.41×10^{-2}	15
Anaphase-promoting complex-dependent proteasomal ubiquitin-dependent protein catabolic process	3.61×10^{-2}	20
Negative regulation of cell migration	3.91×10^{-2}	38
Collagen catabolic process	3.91×10^{-2}	20

Supplemental Table S5. KEGG analysis for the miRNA signature associated with TSS.

KEGG pathway	p-value	Number of Genes
Fatty acid biosynthesis	$1.29E \times 10^{-15}$	6
Proteoglycans in cancer	1.53×10^{-10}	80
Hippo signaling pathway	2.75×10^{-7}	57
Fatty acid metabolism	2.75×10^{-7}	16
Hepatitis B	4.08×10^{-6}	55
Cell cycle	1.49×10^{-5}	55
Adherens junction	2.92×10^{-5}	32
Pathways in cancer	2.92×10^{-5}	132
Viral carcinogenesis	1.68×10^{-4}	65
Endocytosis	1.72×10^{-4}	75
Chronic myeloid leukemia	5.45×10^{-4}	32
Other types of O-glycan biosynthesis	5.47×10^{-4}	10
Colorectal cancer	5.61×10^{-4}	27
ECM-receptor interaction	5.61×10^{-4}	26
Neurotrophin signaling pathway	2.79×10^{-3}	47
Glycosaminoglycan biosynthesis - keratan sulfate	3.07×10^{-3}	6
Bacterial invasion of epithelial cells	3.38×10^{-3}	33
FoxO signaling pathway	3.38×10^{-3}	50
Thyroid hormone signaling pathway	3.38×10^{-3}	44
p53 signaling pathway	3.44×10^{-3}	32
Fatty acid elongation	3.44×10^{-3}	8
Focal adhesion	3.44×10^{-3}	74
Renal cell carcinoma	3.79×10^{-3}	27
Small cell lung cancer	3.79×10^{-3}	36
TGF-beta signaling pathway	3.94×10^{-3}	29
HTLV-I infection	4.76×10^{-3}	86
Transcriptional misregulation in cancer	4.88×10^{-3}	62
Glioma	5.78×10^{-3}	25
Pancreatic cancer	5.78×10^{-3}	29
Lysine degradation	8.17×10^{-3}	18
Bladder cancer	1.06×10^{-2}	19
Epstein-Barr virus infection	1.35×10^{-2}	71
RNA transport	1.52×10^{-2}	57
Chagas disease (American trypanosomiasis)	2.25×10^{-2}	37
Vitamin B6 metabolism	2.70×10^{-2}	3
TNF signaling pathway	3.40×10^{-2}	38
Sphingolipid signaling pathway	3.85×10^{-2}	42
Protein processing in endoplasmic reticulum	3.91×10^{-2}	57
Non-small cell lung cancer	3.97×10^{-2}	23

Apoptosis	4.26×10^{-2}	30
HIF-1 signaling pathway	4.61×10^{-2}	38
Arrhythmogenic right ventricular cardiomyopathy (ARVC)	4.82×10^{-2}	21

Supplemental Table S6. GO analysis for the miRNA signature associated with TSS.

GO category	p-value	Number of Genes
Cellular nitrogen compound metabolic process	5.22×10^{-142}	1242
Biosynthetic process	3.95×10^{-94}	1020
Gene expression	5.06×10^{-80}	239
Cellular protein modification process	1.07×10^{-77}	653
Viral process	3.64×10^{-63}	193
Symbiosis	3.09×10^{-62}	208
Small molecule metabolic process	4.59×10^{-50}	582
Catabolic process	1.36×10^{-49}	513
Biological process	2.93×10^{-41}	3276
Cellular protein metabolic process	8.40×10^{-38}	155
Membrane organization	9.19×10^{-36}	193
Cellular component assembly	1.83×10^{-34}	347
Macromolecular complex assembly	1.83×10^{-34}	259
Mitotic cell cycle	3.38×10^{-33}	134
Neurotrophin TRK receptor signaling pathway	1.32×10^{-31}	94
Nucleobase-containing compound catabolic process	3.51×10^{-31}	253
Response to stress	5.97×10^{-31}	534
Cell death	1.19×10^{-29}	261
Protein complex assembly	1.44×10^{-25}	218
Blood coagulation	4.33×10^{-22}	130
mRNA metabolic process	2.13×10^{-20}	75
Fc-epsilon receptor signaling pathway	7.96×10^{-20}	57
RNA metabolic process	4.87×10^{-17}	79
DNA metabolic process	2.46×10^{-16}	197
Epidermal growth factor receptor signaling pathway	3.70×10^{-15}	70
Cellular component disassembly involved in execution phase of apoptosis	1.79×10^{-14}	26
Post-translational protein modification	2.09×10^{-14}	54
Immune system process	2.55×10^{-14}	349
Chromatin organization	8.67×10^{-14}	52
Cellular lipid metabolic process	7.05×10^{-13}	49
Mitotic nuclear envelope disassembly	7.17×10^{-12}	21
Toll-like receptor TLR1:TLR2 signaling pathway	7.97×10^{-12}	28
Toll-like receptor TLR6:TLR2 signaling pathway	7.97×10^{-12}	28
Toll-like receptor 10 signaling pathway	8.23×10^{-12}	27
Extracellular matrix organization	4.15×10^{-11}	104
Cell motility	6.16×10^{-11}	143
TRIF-dependent toll-like receptor signaling pathway	9.95×10^{-11}	28
Cell junction organization	1.28×10^{-10}	52
Extracellular matrix disassembly	2.07×10^{-10}	39
Transcription initiation from RNA polymerase II promoter	2.28×10^{-10}	68
Toll-like receptor 5 signaling pathway	3.12×10^{-10}	27

Vesicle-mediated transport	3.12×10^{-10}	237
Cytoskeleton organization	6.17×10^{-10}	164
Toll-like receptor 9 signaling pathway	6.17×10^{-10}	28
Platelet degranulation	8.25×10^{-10}	29
Transforming growth factor beta receptor signaling pathway	1.92×10^{-9}	64
Myd88-independent toll-like receptor signaling pathway	1.95×10^{-9}	28
Toll-like receptor 4 signaling pathway	4.10×10^{-9}	34
Toll-like receptor 2 signaling pathway	4.11×10^{-9}	29
Cellular component movement	6.77×10^{-9}	40
G2/M transition of mitotic cell cycle	7.22×10^{-9}	48
Platelet activation	8.02×10^{-9}	55
Toll-like receptor 3 signaling pathway	1.08×10^{-8}	29
Toll-like receptor signaling pathway	1.15×10^{-8}	37
Viral life cycle	1.53×10^{-8}	35
Protein N-linked glycosylation via asparagine	2.34×10^{-8}	34
Protein targeting	3.64×10^{-8}	79
Transcription. DNA-templated	4.08×10^{-8}	510
Regulation of transcription from RNA polymerase II promoter in response to hypoxia	8.99×10^{-8}	15
Fibroblast growth factor receptor signaling pathway	2.41×10^{-7}	53
Glycosaminoglycan metabolic process	2.93×10^{-7}	32
Apoptotic signaling pathway	2.23×10^{-6}	41
Activation of signaling protein activity involved in unfolded protein response	2.72×10^{-6}	22
Nuclear-transcribed mRNA catabolic process deadenylation-dependent decay	3.58×10^{-6}	23
Hexose transport	4.63×10^{-6}	16
Innate immune response	7.79×10^{-6}	150
Myd88-dependent toll-like receptor signaling pathway	8.34×10^{-6}	29
Positive regulation of type I interferon production	9.74×10^{-6}	23
Regulation of ubiquitin-protein ligase activity involved in mitotic cell cycle	9.74×10^{-6}	23
Cell junction assembly	1.19×10^{-5}	21
Cytoskeleton-dependent intracellular transport	1.28×10^{-5}	34
Phosphatidylinositol-mediated signaling	1.54×10^{-5}	38
G1/S transition of mitotic cell cycle	1.71×10^{-5}	50
Regulation of glucose transport	1.78×10^{-5}	14
Positive regulation of ubiquitin-protein ligase activity involved in mitotic cell cycle	2.09×10^{-5}	22
Insulin receptor signaling pathway	2.82×10^{-5}	46
Protein maturation	4.95×10^{-5}	52
SRP-dependent cotranslational protein targeting to membrane	5.29×10^{-5}	34
Axon guidance	5.29×10^{-5}	104
Fc-gamma receptor signaling pathway involved in phagocytosis	5.84×10^{-5}	20
Cell proliferation	6.07×10^{-5}	143
Sulfur compound metabolic process	6.48×10^{-5}	64
Leukocyte migration	6.66×10^{-5}	32
Cell cycle	7.61×10^{-5}	199

RNA splicing	7.82×10^{-5}	80
Nucleobase-containing small molecule metabolic process	8.11×10^{-5}	20
Regulation of defense response to virus by virus	9.61×10^{-5}	12
Post-Golgi vesicle-mediated transport	1.02×10^{-4}	18
Sphingolipid biosynthetic process	1.02×10^{-4}	18
Cell cycle arrest	1.03×10^{-4}	52
DNA damage response. signal transduction by p53 class mediator resulting in cell cycle arrest	1.15×10^{-4}	23
Stress-activated MAPK cascade	1.22×10^{-4}	18
Termination of RNA polymerase II transcription	1.44×10^{-4}	16
Anaphase-promoting complex-dependent proteasomal ubiquitin-dependent protein catabolic process	1.51×10^{-4}	25
Nuclear-transcribed mRNA catabolic process. nonsense-mediated decay	2.01×10^{-4}	36
Nucleocytoplasmic transport	2.01×10^{-4}	82
Ribonucleoprotein complex assembly	2.15×10^{-4}	39
Positive regulation of apoptotic process	2.27×10^{-4}	110
Phospholipid metabolic process	2.97×10^{-4}	41
mRNA processing	3.02×10^{-4}	119
Antigen processing and presentation of exogenous peptide antigen via MHC class II	3.08×10^{-4}	32
In utero embryonic development	3.30×10^{-4}	86
Transcription from RNA polymerase II promoter	3.33×10^{-4}	137
Viral transcription	4.82×10^{-4}	21
mRNA 3'-end processing	7.57×10^{-4}	14
Cellular response to hypoxia	7.61×10^{-4}	43
DNA strand elongation involved in DNA replication	7.70×10^{-4}	12
Positive regulation of transcription. DNA-templated	8.23×10^{-4}	197
Cytokine-mediated signaling pathway	8.95×10^{-4}	70
Notch signaling pathway	8.95×10^{-4}	52
Homeostatic process	1.27×10^{-3}	156
Negative regulation of apoptotic process	1.28×10^{-3}	159
Glycerophospholipid biosynthetic process	1.32×10^{-3}	22
Negative regulation of epidermal growth factor receptor signaling pathway	1.53×10^{-3}	18
Phosphatidylinositol biosynthetic process	1.74×10^{-3}	19
Lipid metabolic process	1.97×10^{-3}	235
Translational termination	2.20×10^{-3}	24
Response to unfolded protein	2.44×10^{-3}	24
mRNA splicing. via spliceosome	2.87×10^{-3}	59
Long-chain fatty-acyl-coa biosynthetic process	2.89×10^{-3}	8
Platelet-derived growth factor receptor signaling pathway	3.24×10^{-3}	21
Ras protein signal transduction	3.46×10^{-3}	30
Activation of MAPKK activity	3.78×10^{-3}	26
Positive regulation of muscle cell differentiation	3.78×10^{-3}	12
Negative regulation of transcription from RNA polymerase II promoter	4.10×10^{-3}	217
Protein polyubiquitination	5.23×10^{-3}	41
Cofactor metabolic process	6.21×10^{-3}	51

Activation of JUN kinase activity	6.78×10^{-3}	19
Negative regulation of transforming growth factor beta receptor signaling pathway	7.01×10^{-3}	30
Apoptotic process	7.20×10^{-3}	185
Muscle cell differentiation	7.25×10^{-3}	16
Intrinsic apoptotic signaling pathway	7.42×10^{-3}	19
Collagen catabolic process	9.19×10^{-3}	21
Generation of precursor metabolites and energy	9.77×10^{-3}	63
Endoplasmic reticulum unfolded protein response	1.13×10^{-2}	32
Transport	1.28×10^{-2}	726
Adherens junction organization	1.32×10^{-2}	14
Dolichol-linked oligosaccharide biosynthetic process	1.32×10^{-2}	12
Inositol phosphate metabolic process	1.32×10^{-2}	12
Negative regulation of cell proliferation	1.38×10^{-2}	124
Positive regulation of I-kappab kinase/NF-kappab signaling	1.74×10^{-2}	60
Notch receptor processing	1.81×10^{-2}	12
Sulfur amino acid metabolic process	1.95×10^{-2}	9
Triglyceride biosynthetic process	2.08×10^{-2}	15
Peptidyl-threonine phosphorylation	2.55×10^{-2}	22
Regulation of small GTPase mediated signal transduction	2.77×10^{-2}	45
Cell-cell junction organization	3.12×10^{-2}	20
Protein stabilization	3.45×10^{-2}	40
Nitric oxide metabolic process	3.70×10^{-2}	8
Erythrocyte differentiation	3.73×10^{-2}	24
Cellular amino acid metabolic process	4.21×10^{-2}	80
Positive regulation of protein insertion into mitochondrial membrane involved in apoptotic signaling pathway	4.25×10^{-2}	9

Figure 1

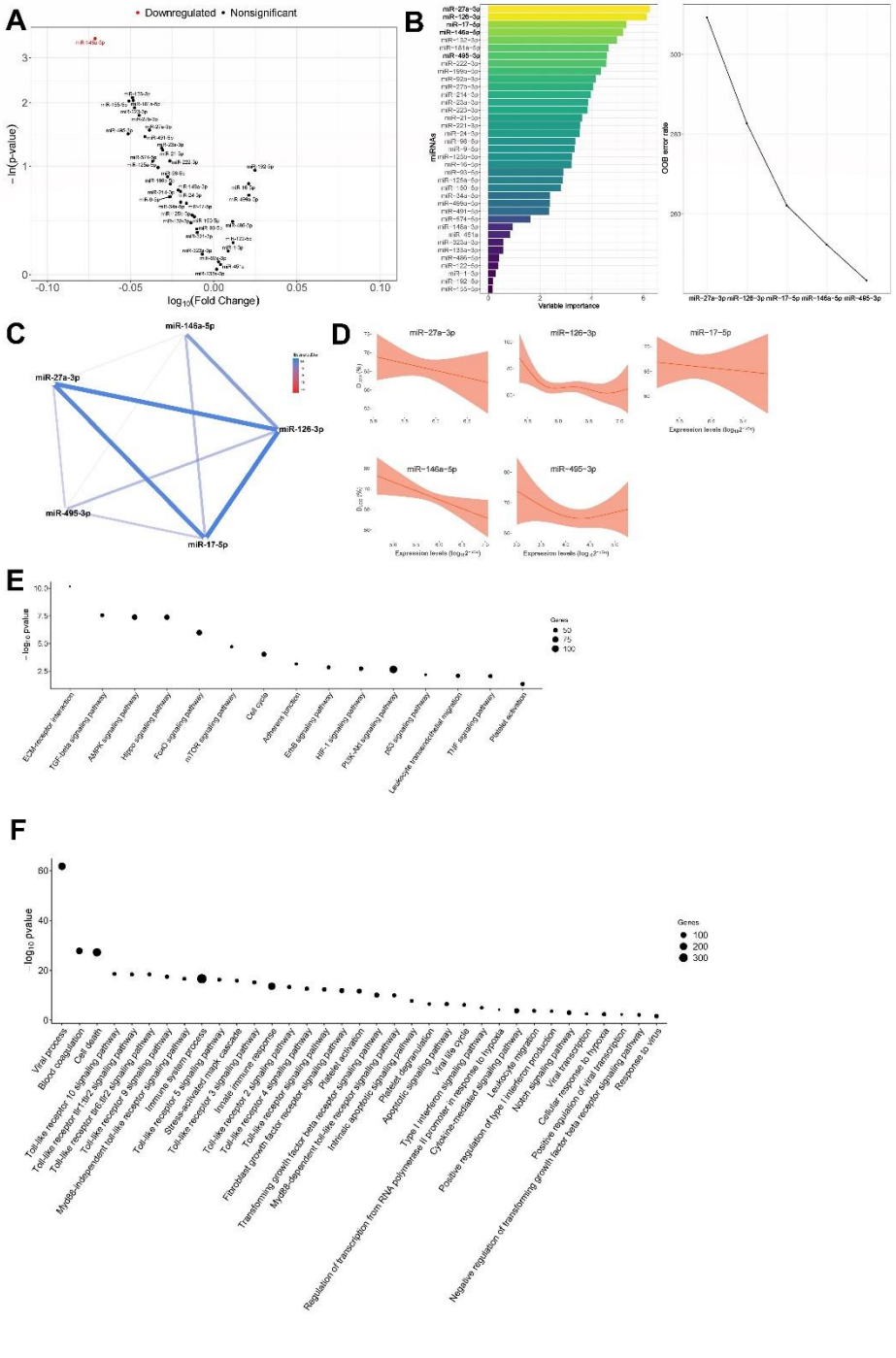

Figure 2

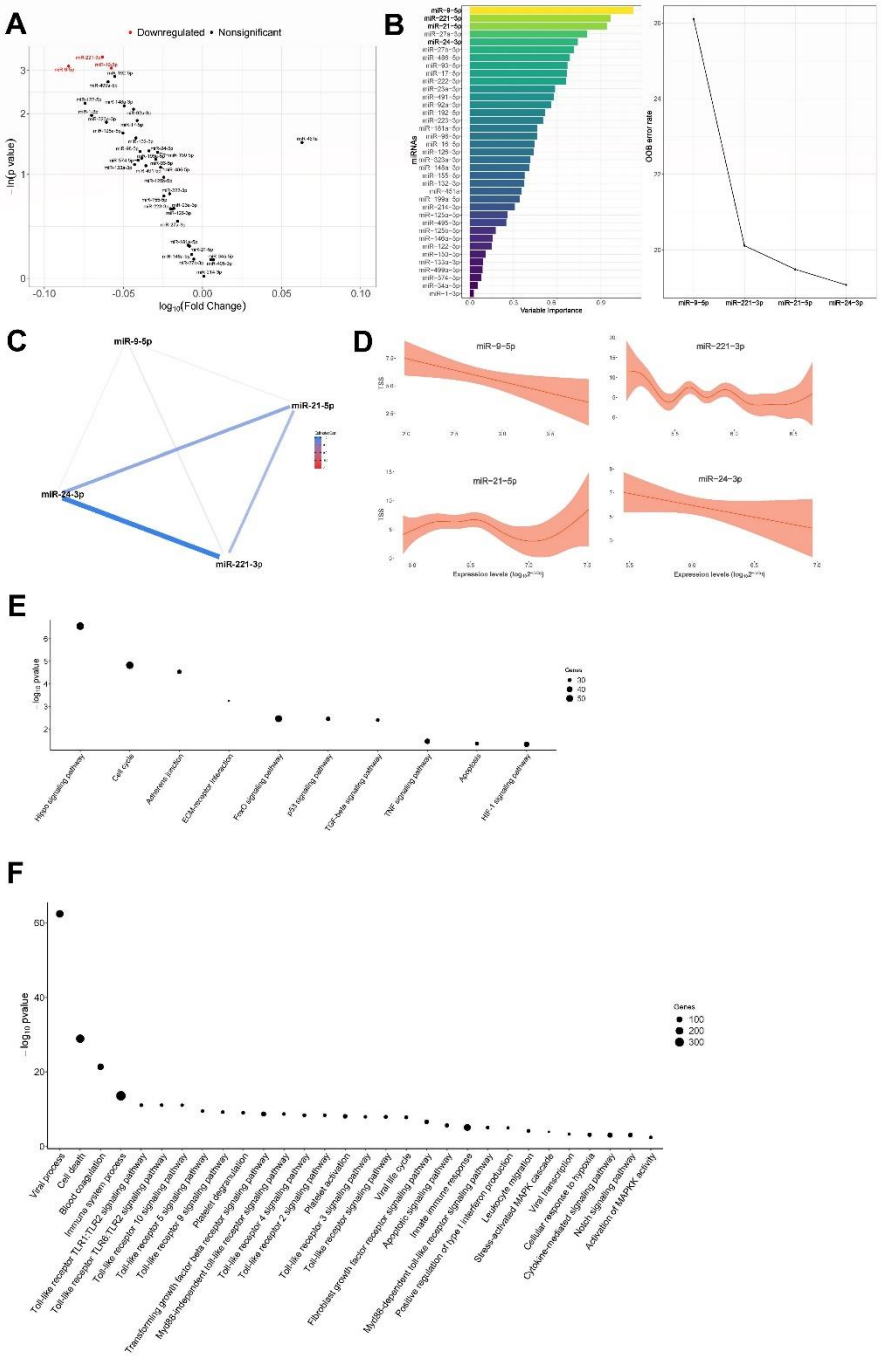
A
Downregulated
Nonsignificant
−ln(p value)
log10(Fold Change)
B
miRNAs
Variable Importance
OOB error rate
miR-9-5p
miR-221-3p
miR-21-5p
miR-24-3p
C
miR-9-5p
miR-21-5p
miR-24-3p
miR-221-3p
D
miR−9−5p
miR−221−3p
miR−21−5p
miR−24−3p
TSS
Expression levels
E
−log10 pvalue
Genes
Hippo signaling pathway
Cell cycle
Adherens junction
ECM−receptor interaction
FoxO signaling pathway
p53 signaling pathway
TGF−beta signaling pathway
TNF signaling pathway
Apoptosis
HIF−1 signaling pathway
F
−log10 pvalue
Genes
Viral process
Cell death
Blood coagulation
Immune system process
Toll−like receptor TLR1/TLR2 signaling pathway
Toll−like receptor TLR6/TLR2 signaling pathway
Toll−like receptor 10 signaling pathway
Toll−like receptor 5 signaling pathway
Toll−like receptor 9 signaling pathway
Platelet degranulation
Transforming growth factor beta receptor signaling pathway
MyD88−independent toll−like receptor signaling pathway
Toll−like receptor 4 signaling pathway
Toll−like receptor 2 signaling pathway
Platelet activation
Toll−like receptor 3 signaling pathway
Toll−like receptor signaling pathway
Viral life cycle
Apoptotic signaling pathway
Innate immune response
Fibroblast growth factor receptor signaling pathway
MyD88−dependent toll−like receptor signaling pathway
Positive regulation of type I interferon production
Leukocyte migration
Stress−activated MAPK cascade
Viral transcription
Cellular response to hypoxia
Cytokine−mediated signaling pathway
Notch signaling pathway
Activation of MAPK activity

Figure 3

A

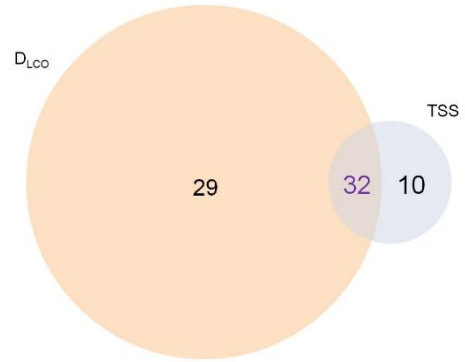

Significant shared KEGG pathways

- Adherens junction
- Cell cycle
- ECM-receptor interaction
- FoxO signaling pathway
- HIF-1 signaling pathway
- Hippo signaling pathway
- p53 signaling pathway
- TGF-beta signaling pathway
- TNF signaling pathway

B

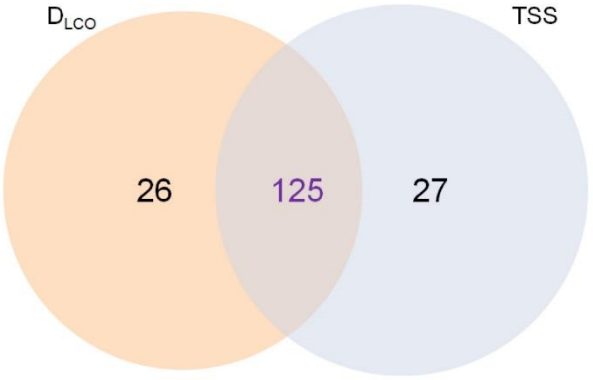

Significant shared GO pathways

- Apoptotic signaling pathway
- Blood coagulation
- Cell death
- Cellular response to hipoxia
- Cytokine-mediated signaling pathway
- Fibroblast growth factor receptor signaling pathway
- Immune system process
- Innate immune response
- Leukocyte migration
- Myd88-dependent toll-like receptor signaling pathway
- Myd88-independent toll-like receptor signaling pathway
- Notch signaling pathway
- Platelet activation
- Platelet degranulation
- Positive regulation of type I interferon production
- Stress-activated MAPK cascade
- Toll-like receptor 10 signaling pathway
- Toll-like receptor 2 signaling pathway
- Toll-like receptor 3 signaling pathway
- Toll-like receptor 4 signaling pathway
- Toll-like receptor 5 signaling pathway
- Toll-like receptor 9 signaling pathway
- Toll-like receptor signaling pathway
- Toll-like receptor TLR1:TLR2 signaling pathway
- Toll-like receptor TLR6:TLR2 signaling pathway
- TGF-beta receptor signaling pathway
- Viral life cycle
- Viral process
- Viral transcription